Transportation Research Part B 189 (2024) 103068

Contents lists available at ScienceDirect

Transportation Research Part B

journal homepage: www.elsevier.com/locate/trb

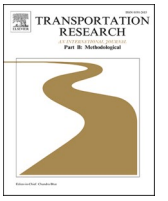

Microscopic Discontinuities Disrupting Hydrodynamic and Continuum Traffic Flow Models

Benjamin Coifman [#]

The Ohio State University, Joint appointment with the Department of Civil, Environmental, and Geodetic Engineering, and the Department of Electrical and Computer Engineering

ARTICLE INFO

Keywords:
Fundamental diagram
Vehicle detection
Traffic flow theory
Hydrodynamic traffic flow model
Continuum traffic flow model

ABSTRACT

This paper explores short duration disturbances in the traffic stream that are large enough to impact the traffic dynamics and disrupt stationarity when establishing the fundamental diagram, FD, but small enough that they are below the resolution of conventional vehicle detector data and cannot be seen using conventional methods. This empirical research develops the Exclusionary Vehicle Aggregation method (EVA) to extract high fidelity time series data from conventional loop detectors and then extends the method to measure the standard deviation of headways in a given fixed time sample, stdevh. Using loop detector data spanning 18 years and five sites, all of the sites show that samples with low stdevh tend towards a triangular FD while samples with high stdevh tend towards a concave FD that falls inside the triangular FD. The stdevh is also shown to be strongly correlated with the duration of the longest headway within the sample. The presence of a long headway means the state is perceptively different over the sample and thus, the measurement is non-stationary. A review of the earliest FD literature by Greenshields finds strong supporting evidence for these trends. Collectively, the loop detector and historical FD results span over 75 years of empirical traffic data.

Based on the EVA analysis, this work offers the following insights: the shape of equilibrium FD appears to be triangular and that conventional detector data mask critical features needed by hydrodynamic traffic flow models, HdTFM. Because the driver behind a long headway can act independent of their leader, the long headways can correspond to unobserved boundary conditions that generate kinematic waves. If these boundaries were detected many HdTFM could accommodate them, especially multi-class models. But the stochastic nature of the long headways also challenges the predictive abilities of deterministic HdTFM. Perhaps the largest of these challenges is driver agency- the driver behind a long headway can maintain it, resulting in signals propagating downstream or they can close the gap, resulting in signals propagating upstream. Meanwhile, this work provides a test for stationary conditions to help ensure an empirical FD supports the assumptions placed upon it.

1. Introduction

Hydrodynamic traffic flow models (HdTFM) and many of the related continuum traffic flow models postulate that the shape of the fundamental diagram (FD) determines the velocity at which signals and characteristics propagate through the traffic stream as

E-mail address: Coifman.1@OSU.edu.
[#] Hitchcock Hall 470, 2070 Neil Ave, Columbus, OH 43210. Phone: (614) 292-4282.

https://doi.org/10.1016/j.trb.2024.103068
Received 12 January 2024; Received in revised form 25 August 2024; Accepted 28 August 2024
Available online 10 September 2024

kinematic waves (KW). Section 1.1 gives a brief overview HdTFM for context. However, the primary focus of this paper is a better understanding of the FD.

The FD relates how the traffic state variables of speed, v, flow, q, and density, k, interrelate as they govern the flow of traffic. Generally, q and v are expressed as functions of k, so in the flow-density plane the FD would typically be defined as: $q = Q(k)$, while $v = q/k$. There is no universal shape of Q(k), but many researchers employ a concave Q(k), $\frac{d^2Q(k)}{dk^2} < 0$, which ensures $\frac{dQ(k)}{dk} < v$ and other desirable properties (e.g., Whitham, 1974; Del Castillo and Benitez, 1995; Li and Zhang, 2011). A triangular shaped Q(k) is also commonly found in the literature (e.g., Drake et al., 1967; Munjal et al., 1971, Hall et al., 1986; Newell, 2002).

Unfortunately, empirical traffic data exhibits considerable scatter, and thus, many different Q(k) curves could be fit to the same set of traffic data and the different curves all have similar levels of error. The real challenge is deriving a meaningful Q(k). To this end, the formulation of the FD should come strictly from stationary traffic states (Del Castillo and Benitez, 1995; Zhang, 1999), Where a stationary traffic state is defined to be homogeneous traffic conditions throughout the entire time-space region of interest, e.g., q and v do not perceptively change at a subsample timescale for the entire duration of a macroscopic sample from a loop detector station (see, e.g., Cassidy, 1998).

This paper empirically explores macroscopic traffic data that gives rise to a smooth, reproducible Q(k) and shows that the macroscopic data can obscure important microscopic dynamics. To study the microscopic dynamics, this paper develops the Exclusionary Vehicle Aggregation method (EVA), a new approach to aggregate traffic data in a manner that eliminates major sources of noise (inhomogeneous vehicle lengths, partial headways) while still grouping many successive vehicles together using a fixed time sampling strategy. It is shown that when the standard deviation of the headways in a sample, σ_h, is low the resulting data exhibit a triangular shaped Q(k). When σ_h increases, the resulting data shows increasing curvature, consistent with a concave Q(k) that falls inside the triangular curve. It is shown that σ_h is strongly correlated with the maximum headway in the sample, i.e., the presence or absence of a large void ahead of a long headway vehicle. These voids are inherently non-stationary because different regions of the sample are perceptively distinct. Although conditions are non-stationary within a macroscopic sample containing a void, if the Q(k) is constructed from samples that contain voids then the emergent trend from the macroscopic data can still yield a smooth, reproducible, concave Q(k) even though it does not represent stationary conditions.

Based on the EVA analysis, this work offers the following insights: the shape of equilibrium FD appears to be triangular and that conventional detector data mask critical features needed by HdTFM. This work represents an empirical case study supporting the need for multi-class HdTFM with mixed regime samples, but it also illustrates challenges that the randomly occurring long headways have on the predictive abilities of deterministic HdTFM and one of the largest challenges is *driver agency*- the driver behind a long headway can maintain it, resulting in signals propagating downstream or they can close the gap, resulting in signals propagating upstream. Finally, this work provides a test for stationary conditions to help ensure an empirical Q(k) supports the assumptions placed upon it.

Table 1
Glossary of terms and variables.

all_lanes	Denotes the case when individual vehicle measurements are combined across all lanes before finding the macroscopic q, k and v.
BHL	Berkeley Highway Laboratory
c	Velocity at which characteristic signals travel via LWR
EVA	Exclusionary vehicle aggregation method for aggregating vehicle detector data
FD	Fundamental diagram
FTS	Fixed Time Sampling- the conventional method for aggregating vehicle detector data
h_i	Headway of i-th passing vehicle
HdTFM	Hydrodynamic traffic flow models
HOV lane	High occupancy vehicle lane
k	Density (veh/mi)
k_j	Jam density (veh/mi)
KW	Kinematic waves
L_i	Effective vehicle length of the i-th passing vehicle- sum of the physical vehicle length and the size of the detection zone
LHV	Long headway vehicle
LWR	Lighthill Whitham and Richards HdTFM
max(h)	Maximum headway in an EVA sample
occ	Occupancy (% time that a detector is occupied)
on_i	Detector "on-time" for i-th passing vehicle
q	Flow (vph)
Q(k)	The FD curve expressed in terms of q as a function of k
s	Spacing between the leading edges of the two loops in a dual loop detector
SHV	Short headway vehicle
Stationary	Homogeneous traffic conditions throughout the entire macroscopic sample, thus, q and v do not perceptively change at a subsample timescale.
SVP	Single vehicle passage method for aggregating vehicle detector data
SwA	Shockwave analysis
σ_h	Standard deviation of headways in an EVA sample
T	Fixed sampling period in FTS and used for grouping vehicles in EVA. Also used as denominator of q and occ in FTS.
T_d	Dynamic sample duration in EVA method, $T_d = \sum retained\_h$ used as denominator of q and occ in EVA, and usually differs from T.
tt_i	Vehicle i's traversal time between the paired loops in a dual loop detector
u	Velocity at which an interface travels via SwA
v	Space mean speed (mph)
v_F	Free speed (mph)

For reference, Table 1 provides a glossary of terms and variables used throughout this paper.

1.1. Hydrodynamic flow

Shockwave analysis, SwA, is probably the oldest continuum traffic flow model. Wardrop (1952) developed SwA showing that the velocity of the interface, u, between abutting states G and H is given by Equation 1. This outcome is a direct result of vehicle conservation, i.e., SwA is simply one manifestation of vehicle conservation between stationary states. In the purest form SwA does not require a FD, it only requires distinct stationary states to exist. When two stationary traffic states abut there must be an interface between them.

$$u = \frac{q_G - q_H}{k_G - k_H} \tag{1}$$

Taking SwA, restricting the set of feasible traffic states to a concave Q(k), and employing an implicit assumption that all of the states on Q(k) are stationary, gives rise to Lighthill Whitham and Richards theory, LWR (Lighthill and Whitham, 1955; Richards, 1956). Under these conditions, as the state evolves it does so by progressing along Q(k) (except during shocks). As a result, the state at any given point in space should be dictated by a KW emanating from one of the region's boundaries. If Q(k) is the same over all time and space, then the KW propagate at velocity c given by Equation 2.

$$c = \frac{dQ(k)}{dk} \tag{2}$$

To illustrate how these theories depend on the FD, consider the concave FD in Fig. 1D, with stationary states G and H highlighted. If these data come from a single lane, the trajectories from state H must be evenly spaced and travel at the same speed, v_H, as per Fig. 1A. If the traffic state transitions via SwA between states G and H on the concave FD, the resulting interface u_{GH} must travel slower than the traffic in ether state G or H. So, vehicles catch up to the interface and change state as they pass it. Whereas LWR predicts that the KW within state H should travel at velocity c_H, where $c_H < v_H$. So, in this case vehicles always overtake the KW and as they do, they adjust their state to match the characteristic at the given point in time and space.

Recognizing that real traffic does not stay on a discrete Q(k), Payne (1971) extended the LWR theory to include a velocity equation that allows for non-equilibrium states that do not fall on Q(k). At this point the HdTFM family tree branches in many directions, a detailed exploration can be found in van Wageningen-Kessels et al. (2015).

The next major advance in HdTFM came with the recognition that different drivers systematically behave differently and their interactions can be too complex to capture with homogeneous vehicles. To this end, multi-class models have emerged in which traffic is modeled as if it were comprised of different vehicle classes, each class with its own distinct behavior (e.g., Daganzo, 2002; Wong and Wong, 2002; Zhang and Jin, 2002; Chanut and Buisson, 2003; Benzoni-Gavage and Colombo, 2003; Logghe and Immers, 2003; Ngoduy and Liu, 2007; Logghe and Immers, 2008; van Lint et al., 2008; van Wageningen-Kessels et al., 2014; Qian et al., 2017).

1.2. Conflicts and limitations

In an empirical study of tunnel traffic, Edie and Baverez (1967) observed that, "small changes in flow may not propagate at a speed equal to the slope of the tangent to a steady-state q-k curve as suggested by the hydrodynamic wave theories of traffic flow. Instead, they are carried along at about stream speed or only slightly less than stream speed right up to saturation flows, at which level they suddenly reverse direction." However, Edie and Baverez did not offer any explanation for the unexpected discrepancy between conventional theory and their empirically observed dynamics. While Zhang, (2002) offers a theoretical explanation for this phenomenon, the topic did not see further empirical examination until Coifman et al. (2023) studied a high occupancy vehicle (HOV) lane that exhibited a concave Q(k) in the free flow regime. Examining data locally at individual loop detector stations, Coifman et al. found that while the macroscopic data yields a smooth, reproducible Q(k), similar to Fig. 1D, the underlying traffic composition appears to be made up of a mix of long headway vehicles (LHV) that act independent of their respective leaders (thus, being able to travel at their preferred speeds) followed by brief queues of short headway vehicles (SHV) that act as if they are strictly operating in the queued regime of a triangular FD. Although across all vehicles the average state resulted in a concave FD, the two distinct populations exhibited their own separate trends, as shown by $Q_{SHV}(k)$ and $Q_{LHV}(k)$ in Fig. 1E. As the traffic speed drops, fewer drivers can maintain their preferred speed, so the percentage of LHV drops and the number of SHV in the moving queues increases. When taking the two groups together, the Q(k) from all vehicles shifts from being close to the LHV trend at high speed towards the SHV trend at lower speeds, giving rise to the concave Q(k), even though the curve is far from representative of either group of vehicles taken individually. The study then measured the velocity at which signals in v and q propagate between successive detector stations and found that although the traffic state fell in the free flow regime of the concave Q(k) the dominant signals appear to travel with the traffic at v, rather than $\frac{dQ(k)}{dk}$ of LWR or $\frac{\Delta q}{\Delta k}$ of SwA.

Coifman et al. found that the microscopic voids ahead of the LHV (bold trajectories in Fig. 1B) and moving queues arising from the moving bottlenecks (lighter trajectories in Fig. 1B) are typically too short to be perceptible in conventional vehicle detector data even though the impacts violate the stationarity assumptions. In this way, the state transitions from state L on the LHV curve to state S on the SHV curve and back again in Fig. 1E, where the dominant state boundaries in Fig. 1B are defined by and travel with the vehicles (what

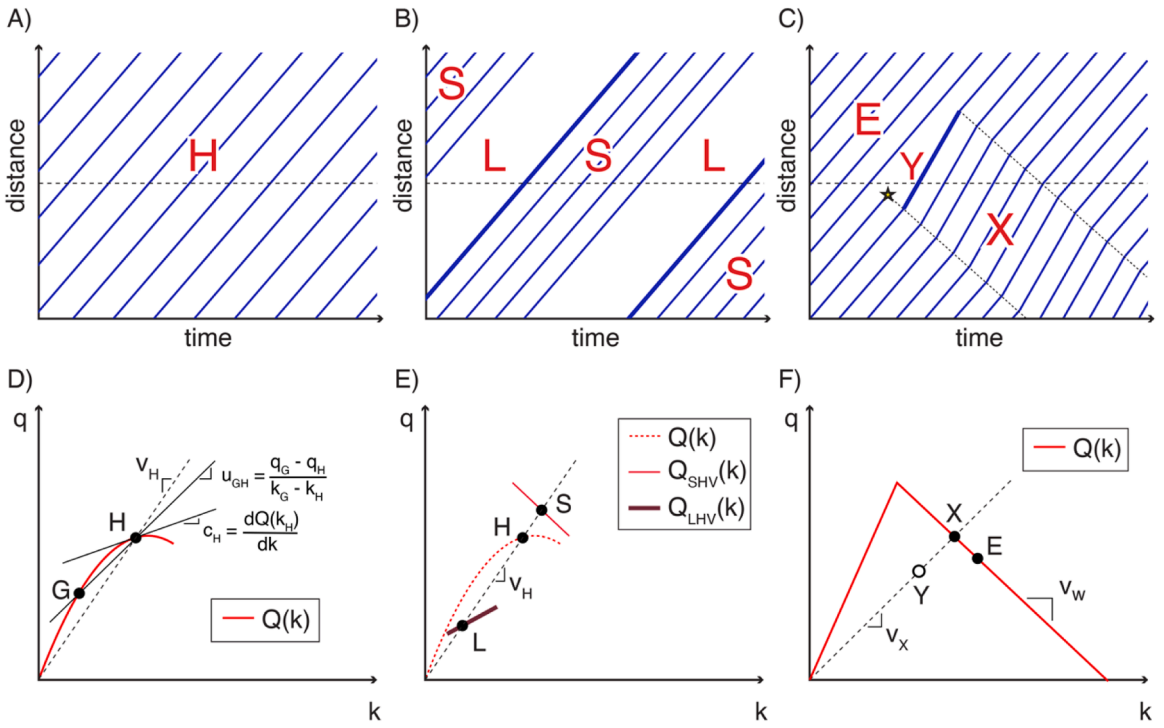

Fig. 1. A hypothetical example showing vehicle trajectories (A) underling a stationary traffic state, (B) non-stationary conditions that yield downstream moving signals that could yield the same macroscopic state as part A, and (C) non-stationary conditions that yield upstream moving signals. (D) A concave FD commonly assumed to hold for HdTFM and the states associated with part A, (B) a concave FD that emerges as the average of two underlying and distinct vehicle groups, each with their own FD, along with the states from part B, and (F) the FD and states associated with part C.

Zhang, 2002, calls "contact discontinuities"). But the duration of states L and S are too short to be isolated in the conventional vehicle detector data, only the average state H is recorded, occluding the non-stationary subsample dynamics that violate SwA and LWR.[1] In this case the voids ahead of the LHV are long-lived, which is why their signals are seen and correlated between successive stations. It is likely that small disturbances form in the moving queues of SHV and propagate upstream, but usually these disturbances are short-lived, dissipating upon reaching the gap ahead of the next LHV.

This general concept of moving bottlenecks disrupting smooth flow is well established in the theoretical literature (e.g., Newell, 1998; Leclercq et al., 2004; Laval, 2009; Duret et al., 2010; Leclercq et al., 2016; Chen and Ahn, 2018), including some multi-class traffic flow models (e.g., Logghe and Immers, 2008) but there are few studies that have examined it empirically (e.g., Munoz and Daganzo, 2002) and we are not aware of any empirical study that has done so on the temporal scale of a detector sampling period. Regardless, as will be shown, these features are both relevant to HdTFM and they are generally below the resolution of conventional vehicle detector data.

The moving bottleneck scenario in Fig. 1B&E adapted from Coifman et al. (2023) is just one example where the macroscopic measurements obscure the non-stationary microscopic dynamics. A vehicle exiting a lane is another example that creates a void, and if the prevailing speed is slower than free speed, it is likely that the void will be short-lived as the following vehicles close the gap. This process is illustrated in Fig. 1C, after a vehicle exits the lane (shown with a star) the following vehicle is briefly unconstrained (as shown with a bold trajectory) as it closes the gap represented by state Y. The gap underlying state Y shrinks as the gap closes, so State Y is shown with an open circle in the flow density plane, Fig. 1F, to indicate the point is not fixed, although speed is constant, the flow progressively increases until the gap disappears. Wang and Coifman (2008) empirically studied these maneuvers in vehicle trajectory data and concluded that the exiting vehicle induced an upstream moving disturbance as the upstream vehicles followed the trajectory of the first vehicle behind the exit, as shown with state X in Fig. 1C&F. They found a median lifetime of 5 sec while the voids are perceptible. But the dominant speeds in that study were below 20 mph. Xuan and Coifman (2012) undertook a similar study using

[1] Throughout this paper, almost all references SwA are in the macroscopic context, i.e., as applied to conventional fixed time averages, and this application can fail if the fixed time average is non-stationary. SwA should still hold when correctly applied at the microscopic scale, as follows: In the presence of a void, instead of transitioning directly from state G to H, SwA transitions from state G to the origin of the flow-density plane and then from the origin to state H, yielding to two signals that travel with the vehicles at the different speeds on either side of the void, rather than the single signal predicted by macroscopic SwA that travels slower than any of the vehicles.

instrumented probe vehicle data and found the median lifetime of 14 sec for a gap behind a departing vehicle, where that study was limited to maneuvers at speeds below 44 mph. At higher speeds it is likely that the lifetimes are longer. In aggregate data, the presence of these short-lived voids will place the average state somewhere in the E-X-Y triangle of Fig. 1F. So in this case the dominant signals should propagate upstream (in contrast to the moving bottleneck example with the dominant signals moving downstream).

In this way, the examples in Fig. 1A-C could all yield the same state measurement from conventional detector data even though part A is stationary and the other two parts are non-stationary. These three scenarios also illustrate an underappreciated challenge to traffic flow modeling: *driver agency:* The LHV driver upstream of a void has a choice between options that change how the traffic state evolves. The driver could maintain the gap resulting in signals moving downstream with their vehicle (e.g., Fig. 1B) at the risk of attracting another vehicle to enter the lane in the gap, or the driver could close the gap resulting in upstream moving signals (e.g., Fig. 1C) while choosing to do so either quickly or slowly. Some of the possible outcomes might be in line with the predictions of a given HdTFM, but a pure HdTFM is deterministic and cannot capture the uncertainty a priori in terms of which outcome the driver will choose.

1.3. Overview

The remainder of this paper develops a method to detect the non-stationary conditions from conventional point detector data. Section 2 reviews both conventional fixed time aggregation and the single vehicle passage methodologies for aggregating loop detector data, then develops the EVA method that incorporates different strengths from the two earlier methods. This section also presents the five dual loop detector data sets used in the analysis. Section 3 uses the EVA method to first explore how the shape of the emergent Q(k) varies in response to the standard deviation of the headways in a given sample, σ_h. Next, it is shown that σ_h is strongly correlated with the maximum headway in the given sample i.e., the presence or absence of a large void. Finally, the paper closes in Section 4 with conclusions.

2. Methodology and Data Sets

This research uses dual loop detector data, and this section presents the details of dual loop detector data aggregation. It begins by reviewing two existing data aggregation methods for context. Section 2.1 covers conventional Fixed Time Sampling and highlights how this method is deficient for developing traffic flow theory. Section 2.2 covers the Single Vehicle Passage method to show how taking a deliberate approach to aggregating the individual vehicle actuations can yield informative insights into traffic dynamics, but these insights come at the cost of taking the vehicles out of sequence and discarding any temporal information.

Section 2.3 develops the new Exclusionary Vehicle Aggregation method, which borrows concepts from the other two aggregation methods to gain additional insights into traffic dynamics and serves as the basis of the analysis in this research. Meanwhile, Appendix A presents some of the finer details of dual loop detector measurements that are not critical to understanding the rest of the paper, but these subtle details are very important for anyone who wishes to reproduce or extend this work. Finally, Section 2.4 presents a brief review of the five loop detector data sets used in this research.

2.1. Conventional fixed time sampling

Most loop dual loop detector stations are configured to collect conventional fixed time sampling, FTS. FTS dates back to Gazis and Foot (1969) if not earlier. The sampling strategy was developed for real time operations, where small sampling errors are not critical, e.g., often an operating agency simply wants to know whether speeds are low or high to produce a three color congestion map. Coifman (2014a) goes into detail as to why FTS is not ideal for advancing traffic flow theory, but usually the individual vehicle actuations are discarded after being aggregated to FTS, leaving no alternatives to FTS in most cases. All of the detector stations used in this study collected the individual vehicle actuations, allowing us to also use the alternative aggregation schemes in the following sections.

At any rate, in the FTS scheme, all samples have the same fixed duration time. Fig. 2 shows a hypothetical example to explain the individual vehicle measurements. Generally, each vehicle is counted in exactly one sample and each speed measurement is attributed to exactly one sample. Ideally both the arrival time and speed measurements from a given vehicle are assigned to the same sample, as will be the case in the present study, but that is not necessarily the case for all dual loop detector deployments. Speed, flow and occupancy are then calculated, e.g., via Equations 3-5, where n vehicles are counted in the given sample.

$$q = \frac{n}{T} \tag{3}$$

$$occ = \frac{\sum time\_detector\_occupied}{T} \cdot 100\% \tag{4}$$

$$v = \frac{n}{\sum 1/v_i} \tag{5}$$

It is important to note that there is no universal standard for calculating FTS, e.g., some operating agencies might calculate time mean speed or truncate occupancy in ways that undermine using the data to understand traffic dynamics (Coifman, 2001). So, care should be taken to understand the specific FTS used in a given data set.

Meanwhile, two of the biggest problems of FTS come from splitting a given vehicle's observations across different samples. Usually,

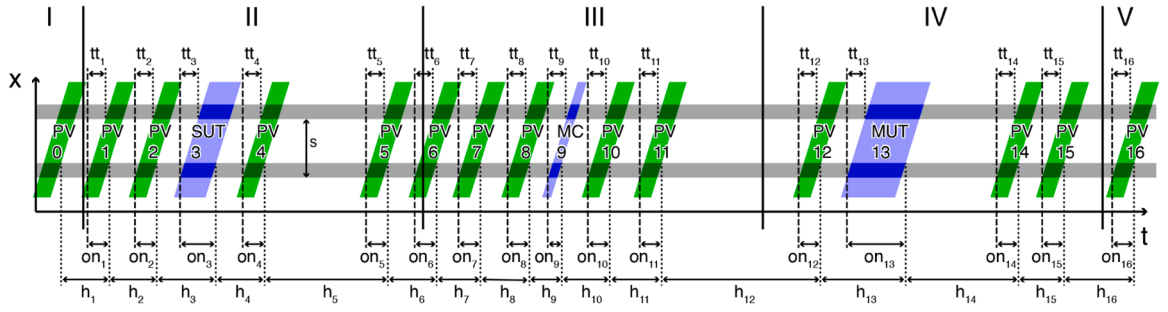

Fig. 2. A hypothetical example showing 17 vehicles passing over a dual loop detector during the span of five fixed time sample periods, numbered I-V. The two loop detectors are shown as horizontal stripes in the time space plane while the vehicle trajectories are plotted to show the physical length of the individual vehicles. The vehicles are numbered from left to right. Veh 3 is a single unit truck (SUT), veh 9 is a motorcycle (MC), veh 13 is a multi-unit truck (MUT), and the remaining 14 veh are passenger cars (PV). For a given vehicle its arrival time is the instant the leading edge enters the upstream detector zone; on-time is the amount of time the vehicle occupies the upstream detector; headway is the time difference between when the vehicle departs the upstream detector and the time the previous vehicle departed the upstream detector; and speed is the quotient of the detector spacing, s, and the traversal time, tt, that it takes the vehicle to travel between the paired detectors.

the headway for the first vehicle in a given sample will fall partially in the previous sample, e.g., vehicle 12 in Fig. 2 arrives in sample IV, but the portion of its headway that falls in sample III is allocated to sample III rather than allocating the entire headway to sample IV in which vehicle 12 is counted. This fractional headway can significantly degrade the fidelity of q for the two samples. On average, the missing fraction of a headway at the start of a sample will be balanced by the added fraction of a headway at the end of the sample, but in any given sample the offset could be far from neutral, leading to considerable noise in q. The second problem comes from splitting a vehicle's on-time across samples. Vehicle 6 in Fig. 2 straddles the boundary between samples II and III. In conventional FTS, the portion of the on-time falling in a given sample is allocated to that sample. In this way, the on-time can be split across samples while the count and speed are allocated to a single sample. As a result, during low flow a sample can have q=0 and occ>0. Additional measurement noise comes from the relatively small number of vehicles seen in a sample and aggregating vehicles of different lengths together, e.g., a truck will contribute a much larger on-time than a passenger vehicle traveling at the same speed (see, e.g., Coifman and Neelisetty, 2014).

2.2. *Single vehicle passage methodology*

The Single Vehicle Passage, SVP, methodology for aggregating dual loop detector data was developed to isolate and extract finer details of traffic dynamics. The SVP method was designed to minimize the sampling errors from FTS and ensure large samples of homogeneous vehicles. For each single vehicle passage, the flow, q_{svp}, occupancy, occ_{svp}, speed, v_{svp}, and effective length, L_{svp}, are calculated via Equations 6-9 (Coifman, 2014b), thereby avoiding the split headways and on-times of FTS. Where h is the headway of the vehicle measured rear bumper of the previous vehicle to the rear bumper of the current vehicle to ensure that the gap ahead of the current vehicle is associated with that vehicle since ultimately a given driver controls the gap ahead of themself. On-time, on, is the time for which the vehicle occupied the upstream detector; detector spacing, s, is the distance between the leading edge of each loop of the dual loop detector; and the traversal time, tt, is the difference between the actuation times at the downstream and upstream detectors.

To ensure homogeneous vehicle samples, instead of grouping vehicles based on their arrival order, SVP bins vehicles by their length and then their speed. At this point, any individual bin with fewer than 100 vehicles is discarded to ensure the sample sizes are sufficiently large enough to be representative. For the remaining bins the median speed, flow and occupancy are found. Because the samples have homogeneous vehicle length, the measurements can also be used to calculate density for the given bin via $k = q/v$, and average vehicle spacing from the reciprocal of k (Coifman, 2015).

$$q_{svp} = \frac{1}{h} \tag{6}$$

$$occ_{svp} = \frac{on}{h} \cdot 100\% \tag{7}$$

$$v_{svp} = \frac{s}{tt} \tag{8}$$

$$L_{svp} = v_{svp} \cdot on \tag{9}$$

The SVP method is very different from FTS, the SVP data are collected over an extended period (typically ranging from one day to several months) and it is only after all of the data have been binned that any aggregation is done. In the case of SVP, Fig. 2 would represent a very small portion of a given sample. Since all vehicles are binned by length the two trucks and one motorcycle would be

sorted into their respective length bins. If one wants to study these less common vehicle lengths the data set needs to be very large to ensure the respective speed bins are above the 100 observation threshold. Assuming the remaining 13 vehicles all have lengths falling in the 18 to 22 ft range, they all go into the same length class and then are sorted by speed into their respective bins. In this way, to achieve homogeneous vehicle lengths and speeds the arrival order and times are completely discarded. The SVP provides a low noise measure of the central tendency of the vehicle data, often the data yields well defined curves for a given vehicle length bin without any smoothing across the independent speed bins.

Various studies have extended the SVP to compare different conditions by adding another dimension to the binning, e.g., adjacent lane speed, time of day, flow, and headway (Ponnu and Coifman, 2015 & 2017; Coifman and Ponnu, 2020). These comparison studies have revealed previously unknown dependencies, e.g., adjacent lane speed modulating driver behavior and the FD in the ego lane.

2.3. Exclusionary vehicle aggregation methodology

Both FTS and SVP predate this work. To capture the temporal evolution of the traffic state from FTS with the noise suppression of SVP, this paper introduces the Exclusionary Vehicle Aggregation, EVA, methodology. Like SVP, the traffic state is measured for each vehicle as it passes the dual loop detector: speed; headway, h (rear bumper to rear bumper); detector on-time, on; and vehicle length via Equations 6-9. But like FTS, the vehicles are binned into successive fixed time arrival windows (successive T=30 sec in this study). Unlike conventional fixed time sampling, the vehicle brings its entire headway. So, the observation time allotted to a given sample is dynamic and will vary from the fixed time arrival window used to assign vehicles to samples. By definition the sample will have an integer number of headways, and all of the measurements from a given vehicle are allocated to a single sample. For this work each vehicle is assigned to the sample in which it first enters the upstream loop detector.[2] Next, recognizing that the different vehicle lengths have different dynamics (Coifman, 2015), only passenger vehicles are retained for this study (18-22 ft veh, which comprise roughly 70% of the passing vehicles in the data sets used herein), with all other vehicles excluded from the aggregated state calculation (hence the name EVA).[3] Note that the headways for the retained vehicles do not change, the aggregation simply skips over the excluded vehicles. The discarded trucks and motorcycles reduce the number of vehicles in the sample but since their positions in the sequence of vehicles are random, the impact of their removal should be unbiased. In this manner the EVA method can be applied to an individual lane or all lanes combined at a given detector station. The latter condition is henceforth denoted "all_lanes," where all vehicles that pass during the given sample, regardless of lane, are aggregated together for that sample.

In each sample speed, flow and occupancy are calculated using only the N retained vehicles (i.e., those with $18 \leq L_{svp} \leq 22$ ft) via Equations 10-15 for the given fixed sample period using a dynamic sampling duration T_d via Equation 11. In this way, T_d is the sum of the headways from all of the retained vehicles in the sample and thus, T_d varies on a sample by sample basis. Meanwhile, for the first and last vehicles in the sample a portion of their h_i and on_i used in the EVA calculations might occur outside of the arrival window period.[4] So in the EVA method traffic is still sampled every fixed T, but the actual time allotted to the calculations for that sample is dynamic T_d, where T_d could be smaller or larger than T, depending on the passage times of the vehicles bounding the start and end of T and the lengths of the observed vehicles. Like the SVP method, because the samples have homogeneous vehicle length, the EVA measurements can also be used to calculate density via Equation 15 (Coifman, 2015).[5]

$$N = number\ of\ 18 \leq L_{svp} \leq 22\ \text{ft}\ vehicles\ passing\ during\ T \tag{10}$$

$$T_d = \sum_{i=1}^{N} h_i \tag{11}$$

$$q = \frac{N}{T_d} \tag{12}$$

$$occ = \frac{\sum_{i=1}^{N} \text{on}_i}{T_d} \cdot 100\% \tag{13}$$

$$v = \frac{N}{\sum_{i=1}^{N} 1/v_i} \tag{14}$$

$$k = q/v \tag{15}$$

In this paper we use EVA to generate Q(k). To remove the impacts of low flow free flow conditions (where HdTFTM do not apply), in

[2] The specific event used for assigning vehicles to samples is not critical provided it is consistent across all vehicles, e.g., one could just as easily use the time a vehicle departs the downstream loop detector to assign all vehicles to a given sample period.

[3] Obviously, the range of retained vehicle lengths may need to be adjusted when applying EVA to a different data set,

[4] An extreme example often occurs during the early morning hours, where it is possible for a vehicle to have $h_i \gg T$.

[5] In the case of EVA, Equation 15 only applies when the traffic state in the sample is stationary, but as will be shown in Section 3.1, the presence of microscopic voids can disrupt stationarity. As is commonly employed in the literature, the equation should become *approximately equal* when the traffic state is sufficiently *near-stationary*.

this paper all samples with fewer than five retained vehicles are also excluded to minimize the noise from small samples.[6] Whereas in other applications (e.g., time series analysis) one would likely want to keep those samples. Also note that throughout this paper we exclude samples with speeds below 10 mph. The conventional speed-trap measurement of Equation 8 assumes acceleration is negligible, but as per Wu and Coifman (2014), for measured speeds below 10 mph one cannot ignore the impacts of acceleration when measuring speed at a dual loop detector.

To illustrate the basic EVA approach using the hypothetical example in Fig. 2, vehicles 1-6 are assigned to sample II, vehicles 7-11 are assigned to sample III, and vehicles 12-15 are assigned to sample IV. In the process, vehicles 3, 9 and 13 are discarded because they fall outside of the passenger vehicle length range. Using the minimum number of five vehicles per sample, only sample II would be retained as having enough vehicles, with N = 5. The resulting state for sample II is given by Equations 16-19, note that vehicle 3 (a long truck) has been excluded from all of the calculations.

$$T_d = h_1 + h_2 + h_4 + h_5 + h_6 \tag{16}$$

$$q = \frac{5}{T_d} \tag{17}$$

$$occ = \frac{on_1 + on_2 + on_4 + on_5 + on_6}{T_d} \cdot 100\% \tag{18}$$

$$v = \frac{5}{1/v_1 + 1/v_2 + 1/v_4 + 1/v_5 + 1/v_6} \tag{19}$$

To illustrate the methodology using real data, we apply EVA to the individual loop detector actuation data set from Coifman (2015) using a 30 sec sampling period. For each lane the resulting scatter plot of the individual measurements is a large cloud of points in the flow-density plane, qk (not shown). For each lane taken individually we bin all of the EVA samples by speed, find the median q, k and v across all of the EVA samples in a given speed bin and then connect the results from the independent speed bins into a curve without any smoothing between bins. This process is then repeated for all five lanes taken together. Any bin with fewer than 50 observations is discarded, the remaining bins are retained and used as the resulting Q(k), as shown in Fig. 3A. Note that no smoothing has been applied to the curves and the samples underlying any point in a given curve is independent of the samples underlying any other point in that curve. Unfortunately, the qk plane visually compresses higher speeds in a small area, so Fig. 3B projects these curves into the speed-flow plane, vq. It is clear from Fig. 3B that the curves span the range of speeds from 10 to 70 mph, with the excluded 0 to 10 mph taking up roughly half of the physical space in Fig. 3A. These plots (and most other plots in this paper) show dashed curves for reference at constant v for 10, 40 and 65 mph, and for u emanating from k_j at -10 and -18 mph. Lane 1 is a time of day HOV lane, and so it exhibits two separate peak flows in Fig. 3B: the higher speed peak coming from non-HOV hours and the lower speed peak during HOV hours.[7]

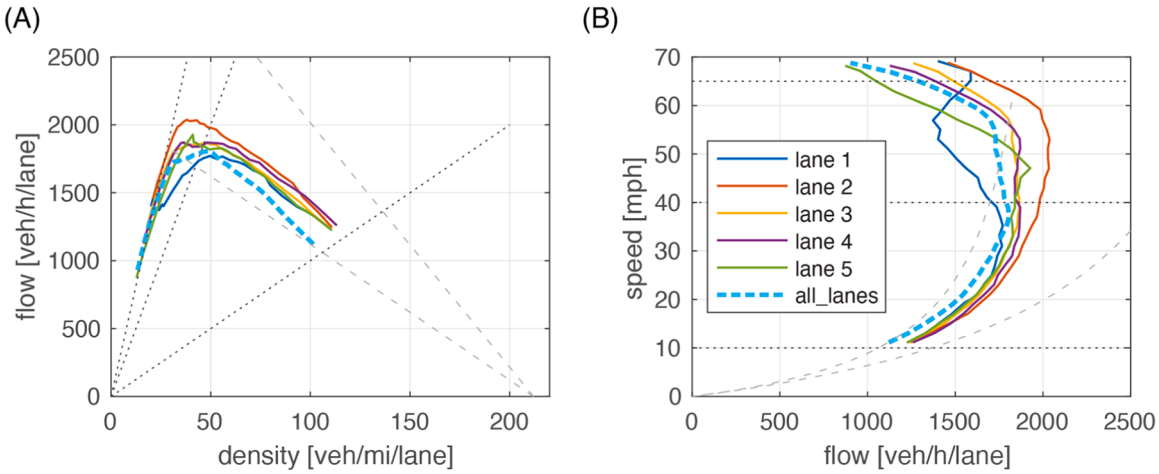

Fig. 3. Curves showing the median EVA (q,k,v) in each speed bin for each lane and all_lanes for the BHL eb 2000 data set, (A) in the flow-density plane, and (B) the speed-flow plane. Throughout, dashed curves are shown for reference across the plots at constant v = 10, 40 and 65 mph, and u = -10 and -18 mph.

[6] Although not shown in the paper, the analysis was repeated without the five vehicle per sample threshold and the general trends seen in Section 3.1 are similar.

[7] See Ponnu and Coifman (2015) and Coifman et al. (2023) for details on how HOV operations impact the FD at this site.

All other lanes exhibit a well-defined concave Q(k), with flows peaking between 40 and 50 mph in most lanes, the same is true for the case of all_lanes combined. As Section 3.1 will show, the concave Q(k) is typical of the sites studied in this work.[8]

While the general concepts underlying EVA are straight forward, the success of the method depends on the quality of the raw data. To this end, Appendix A presents some of the finer details of dual loop detector measurements that are not critical to understanding the rest of the paper, but these subtle details are very important for anyone who wishes to reproduce or extend this work.

2.4. Empirical dual loop detector data sets

The first data set comes from seven dual loop detector stations in the eastbound lanes of I-80 in Emeryville and Berkeley, CA in the Berkeley Highway Laboratory, BHL (Coifman et al., 2000). These data were collected over 29 days in April 2000, they include over 21 million vehicle passages, and will be called BHL eb 2000.[9] For this research we studied: (i) each lane at each of the stations individually, (ii) all_lanes at each station combined, (iii) each lane at all stations pooled, and (iv) all_lanes at all stations pooled. As per above, at a given station, for all_lanes combined: all vehicles that pass in any lane during the given sample are aggregated together, whereas for all stations pooled each station is processed independently and then all of the station results are collected into a single pool.

While the results differed by lane, the general trends were similar across each station taken individually. So for brevity we present the BHL eb 2000 results from iii & iv. We have already presented some of the results from this data set in Fig. 3. The second data set comes from seven stations in the westbound lanes of the BHL over 31 days in October 2003, and will be called BHL wb 2003. Like the first data set, we present the results from iii & iv. The third data set comes from westbound station 103 on I-70/71 in Columbus, Ohio, consists of 67 days between August 2008 and November 2011, and will be called CMFMS wb 2008.[10] Since only one station is used, we present the results from i & ii. The fourth data set comes from one station on eastbound I-80 in Pinole, CA. These data were collected over 97 days between November 2010 and March 2011 and will be called Pinole eb 2010. Once more, because only one station is used, we present the results from i & ii. The final data set comes from the Freeway Service Patrol study (Skabardonis et al., 1996) at seven dual loop detector stations[11] along southbound I-880 in Hayward, California over 49 days between February and October 1993, and will be called FSP sb 1993. Like the first data set, we present the results from iii & iv. Collectively, these loop detector data sets were collected over a span of more than 18 years.

For all of the data sets lane 1 is the inside or passing lane on the left and the numbering increases successively as one moves to the shoulder on the right. At all sites except CMFMS wb 2008, the speed limit is 65 mph and lane 1 is a time of day HOV lane that aside from the HOV diamond markings and signage was marked as if it were a normal general purpose lane. Meanwhile, at CMFMS wb 2008 the speed limit is 55 mph and all of the lanes there are strictly general purpose lanes. At all of the sites the legal rule of the road is for slower traffic to keep right, so the effective free speed exhibited by the traffic usually drops in each successive lane as one moves from lane 1 to lane 5.

Typically, the free flow regime at a given location exhibits a roughly constant free speed over a wide range of flow. This fact can undermine the results when binning by speed. So for the loop detector data we will exclude the highest speeds from the calculations, as follows. First, it is recognized that the free speed, v_F, varies by lane. In the fast lane v_F likely exceeds the speed limit while in the slowest lane it might fall below the speed limit. Lee and Coifman (2012b) showed that the daily median speed provides a good measure of v_F in a given lane. For the present study, in each lane we set v_F to either the speed limit or the daily median speed, whichever is lower. Then, we exclude all speed bins where $v > v_F - 5mph$.

3. Analysis

It is difficult to derive to a clean Q(k) from empirical traffic detector data due to sampling errors (Coifman, 2014a) and the fact that real traffic exhibits a wide range of behavior. No matter how individual measurements of q and k (or occ) are made, a scatter plot of the individual measurements result in a large cloud of points in the qk plane (e.g., the outer envelope of points in Fig. 4C). As a result, many different curve shapes can be fit to the data with similar levels of error (see Coifman and Kim, 2011 for further discussion). As per Section 2.3, in using the EVA method to establish Q(k) we take each lane individually, bin all of the EVA samples by speed, find the median q, k and v across all of the EVA samples in a given speed bin and then connect the results from the independent speed bins into a curve without any smoothing between bins. This process is then repeated for all_lanes combined. Section 3.1 extends the EVA method to explore how the shape of Q(k) changes in response to the underlying headways. With these new insights in mind, Section 3.2 reviews the earliest FD literature and reveals evidence in these classic papers that supports our findings from the loop detector data. Collectively, the loop detector and historical FD results span over 75 years of empirical traffic data.

[8] Note that the FD generated by EVA method might differ significantly from the FD generated by the SVP method as applied to the same data set, e.g., Fig. 3 shows a concave FD via EVA but using the same data Coifman (2015) generated a triangular FD via SVP. If there is a minority of LHV in the traffic stream, the SVP will be insensitive to their presence because it finds the median from hundreds or thousands of vehicles in a single bin whereas the EVA finds the average in each sample. Since a given sample might only include a few vehicles just one LHV in an EVA sample could have a large impact on the sample's average.

[9] These data are from Coifman (2015) and are available at Coifman (2024)

[10] A portion of this data set was released with Wu and Coifman (2019).

[11] Specifically, the seven successive stations in the four lane segment: 19, 13, 12, 4, 17, 15, 5.

3.1. Results from EVA

As noted previously, stationarity is defined as homogeneous traffic conditions throughout the entire macroscopic sample, thus, q and v do not perceptively change at a subsample timescale. Like the SVP method, the EVA method can be extended to bin by additional dimensions. In this work, recognizing the impact of voids on the stationarity of a macroscopic sample, the EVA method is extended to classify each sample by the standard deviation of the headways that were included in the sample, σ_h, thereby quantifying the homogeneity of the sample's underlying vehicle headways. In this way, the extended EVA first bins the samples into four successive ranges of σ_h before binning each of them by speed.

3.1.1. A family of curves

Returning to the BHL eb 2000 data set (previously seen in Fig. 3), we now apply the extended EVA with σ_h thresholds at 0.6, 0.9 and 1.2 sec to sort the data into four σ_h bins. The cloud of points in Fig. 4A shows the resulting EVA flow-density measurements from lane 3 at all seven stations for all samples with $\sigma_h < 0.6s$. The curve shows the median q and k for each 2 mph speed bin between 12 and 60 mph, and any bin with fewer than 50 samples is excluded. The curve shows the median for each bin, without any smoothing between bins, and traces out an almost textbook example of a triangular Q(k).[12] Fig 4B repeats the comparison, only now using strictly the samples with $\sigma_h > 1.2s$. For the higher σ_h a concave Q(k) emerges. The flow-density plane visually compresses the speed range over which the transition occurs. To highlight how the qk plane compresses higher speeds, a thin curve is used for speeds below 25 mph and a thicker curve for speeds above 25 mph, showing that the lowest 1/3 range of speeds consumes more than 1/2 of the physical length of the curve. As before, the plots show dashed curves for reference at constant v for 10, 40 and 65 mph, and for u emanating from k_j at -10 and -18 mph.

Fig. 4D-E show the same data in the speed-flow plane, and it is evident that for the Q(k) created from the samples with $\sigma_h > 1.2s$, q decreases with v for speeds above 40 mph, i.e., the free flow regime spans v > 40 mph. Whereas, for the Q(k) created from the samples with $\sigma_h < 0.6s$, q continues to increase with v throughout the entire range, i.e., the free flow regime does not begin until some point above 60 mph.

Of course, binning by speed like this eliminates any meaningful insights for the free flow regime of a triangular Q(k) since all q at free flow should have roughly the same v, which is why we terminate the curves when $v > v_F - 5mph$. Fig. 4C&F superimpose the

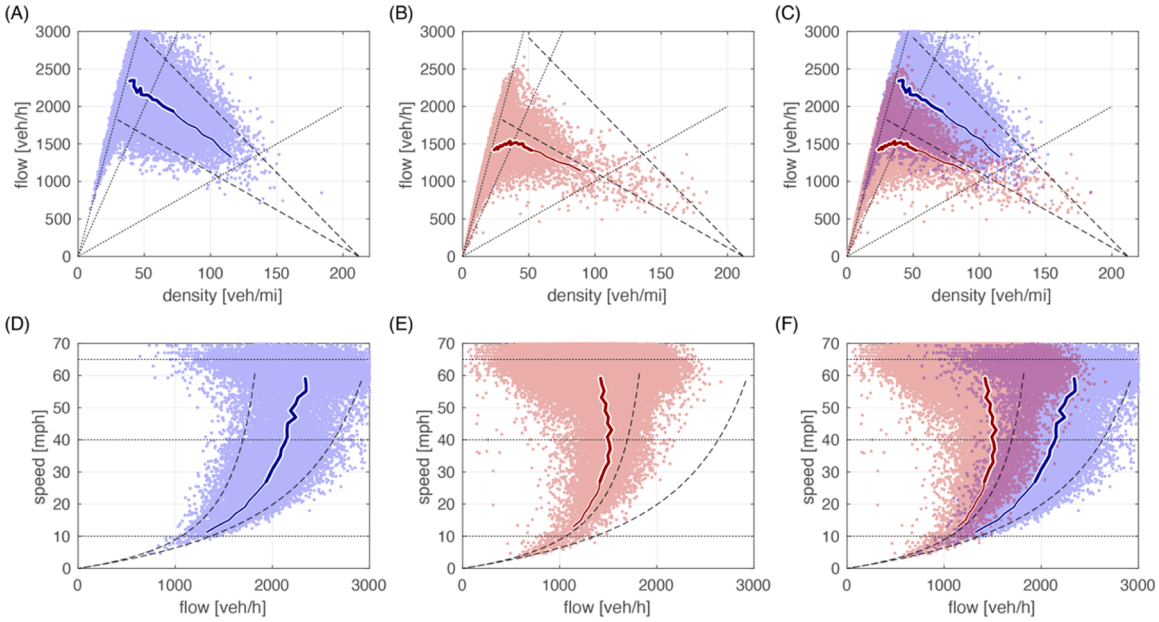

Fig. 4. Extended EVA results for Lane 3 in the BHL eb 2000 data set. First in the flow-density plane with the raw EVA measurements and a curve showing the median (q,k,v) for each speed bin for (A) $\sigma_h < 0.6s$, (B) $\sigma_h > 1.2s$, and (C) both combined. Bins above 25 mph shown with a thicker line. The same data presented in the speed-flow plane, (D) $\sigma_h < 0.6s$, (E) $\sigma_h > 1.2s$, and (F) both combined. Throughout, dashed curves are shown for reference across the plots at constant v or u.

[12] Recall from Section 2.3 that all samples with fewer than five retained vehicles are excluded to minimize the noise from small samples. This decision was made in part because σ_h for a sample of one vehicle is zero, which has the impact of pulling the lowest σ_h bin to lower q at free flow speeds. The other σ_h bins were unaffected by the single vehicle samples because they have a minimum σ_h>0.

previous plots to facilitate comparison. In the process, these plots demonstrate the benefit of presenting the data in the speed-flow plane: the divergence between the curves becomes much clearer in Fig. 4F where the conditions at higher speeds are not compressed relative to those at lower speeds. Meanwhile, Fig. 4C also illustrates the importance of binning by speed rather than density: when k falls between 20 and 50 veh/mi a density bin can include both high flow congestion (Fig. 4A around 60 mph) and low flow free flow states (Fig. 4B around 40 mph).

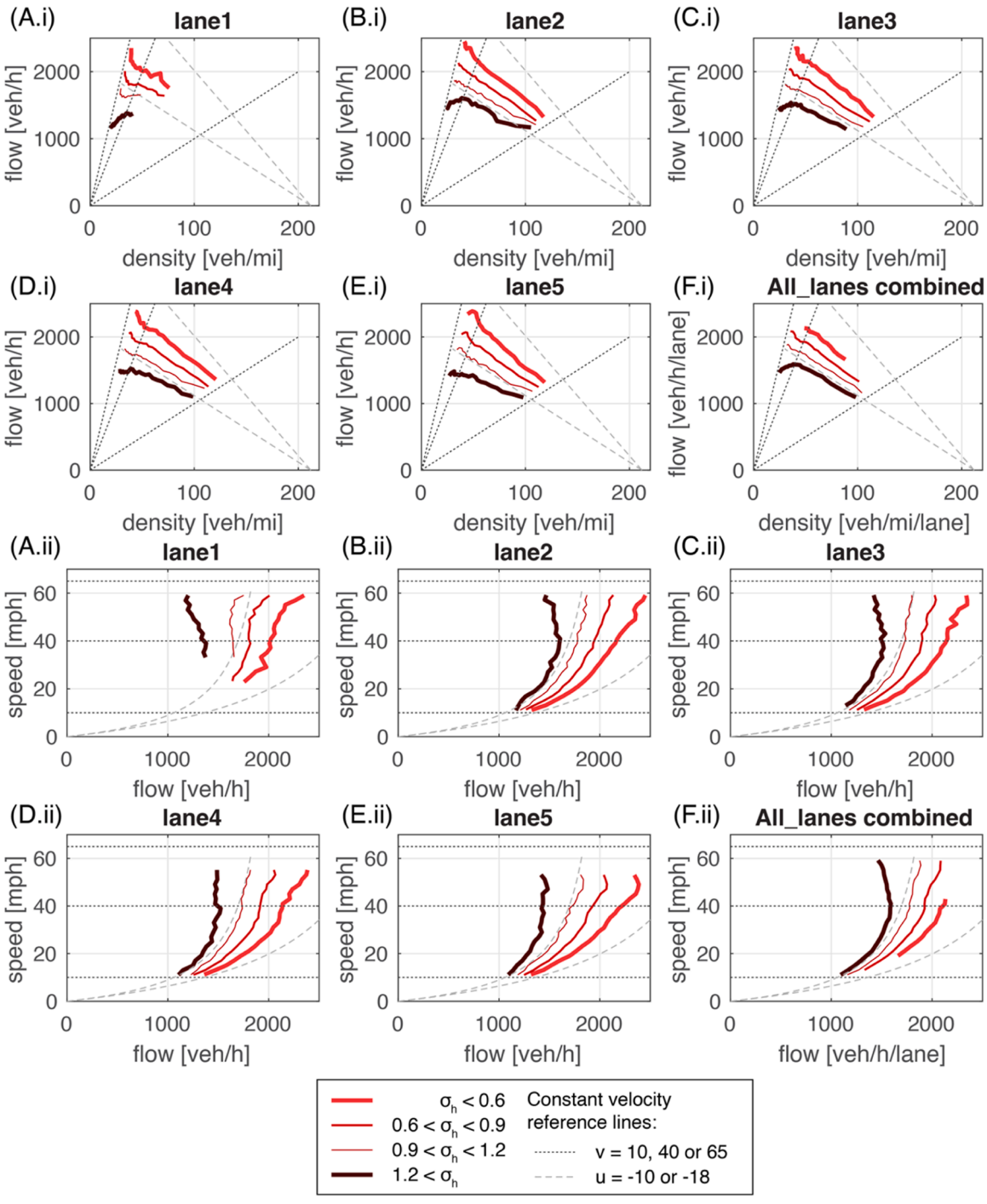

Fig. 5. Curves showing the median EVA (q,k,v) in each speed bin from the BHL eb 2000 data set for the four different σ_h bins in (A) Lane 1 to (E) lane 5, and (F) all_lanes combined. The top two rows of subplots denoted with .i show the flow-density plane where σ_h increases from the top curve to bottom, while the bottom two rows of subplots denoted with .ii show the exact same data in the speed-flow plane, now σ_h increases from right to left. Throughout, dashed curves are shown for reference across the plots at constant v or u.

As σ_h of the samples increases the shape of Q(k) transitions from triangular to concave. Trouble is, σ_h varies from sample to sample, so one cannot count on the state falling on Fig. 4A, Fig. 4B, or either of the two intermediate σ_h bins (not yet shown) at any given time. These results are not limited to lane 3, Fig. 5 repeats the comparisons for each of the five lanes taken individually and all_lanes combined. Now the cloud of individual measurements has been suppressed for clarity, with only the median curves shown for each σ_h bin and the two intermediate bins have now been added to show the progression. The subplots in this figure show: (A) Lane 1 to (E)

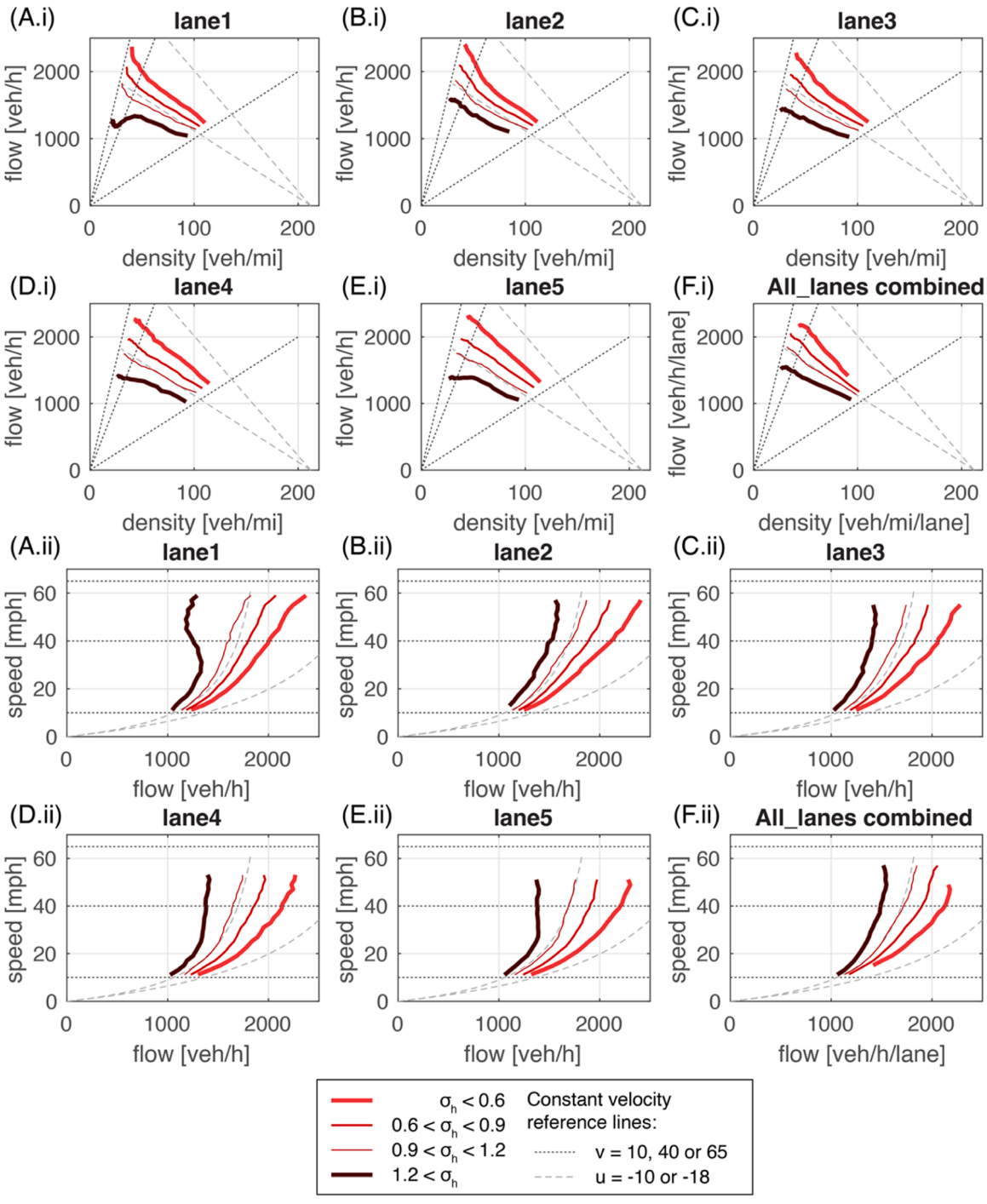

Fig. 6. Curves showing the median EVA (q,k,v) in each speed bin from the BHL wb 2003 data set for the four different σ_h bins in (A) Lane 1 to (E) lane 5, and (F) all_lanes combined. The top two rows of subplots denoted with .i show the flow-density plane where σ_h increases from the top curve to bottom, while the bottom two rows of subplots denoted with .ii show the exact same data in the speed-flow plane, now σ_h increases from right to left. Throughout, dashed curves are shown for reference across the plots at constant v or u.

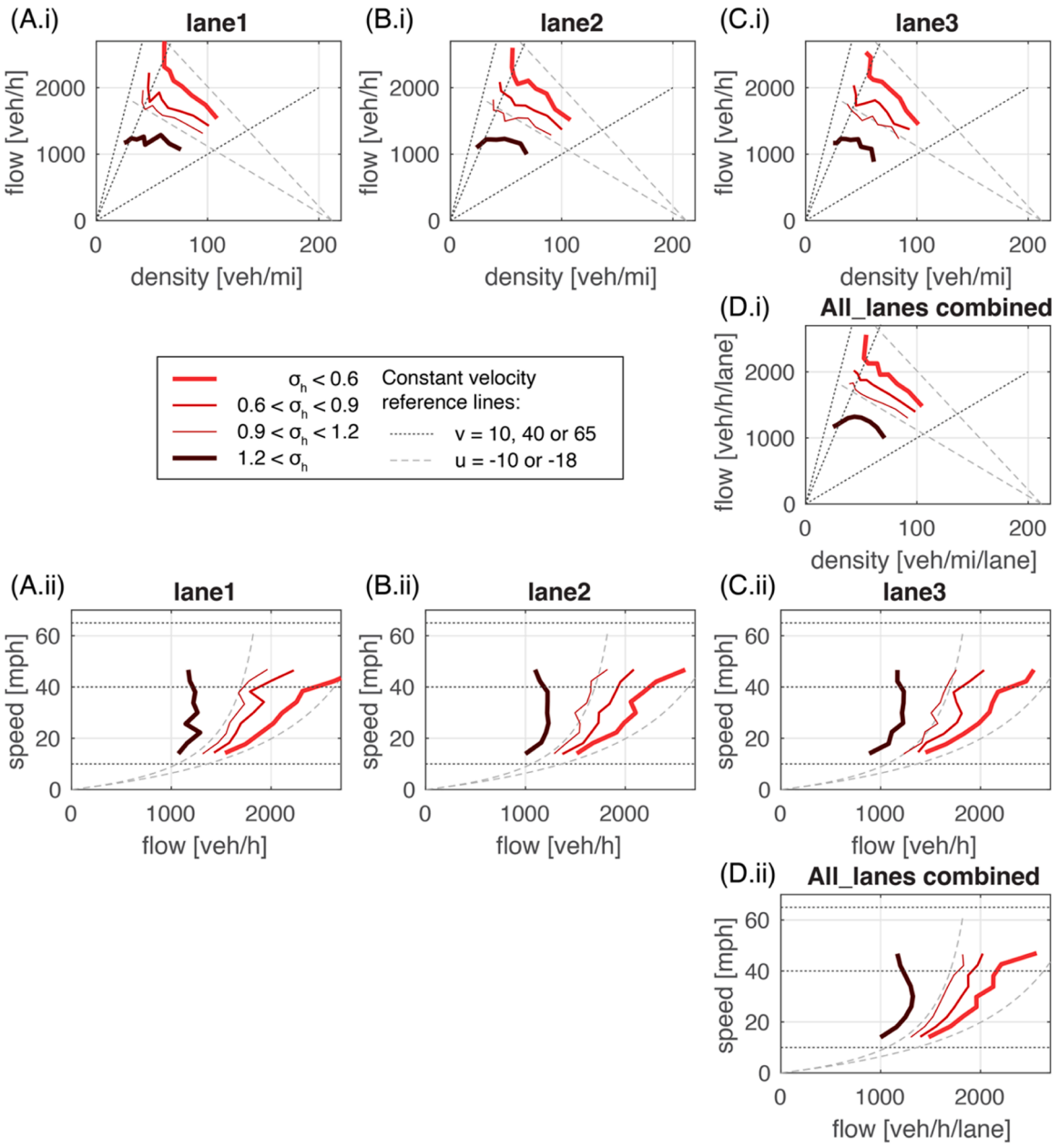

Fig. 7. Curves showing the median EVA (q,k,v) in each speed bin from the CMFMS wb 2008 data set for the four different σ_h bins in (A) Lane 1 to (C) lane 3, and (D) all_lanes combined. The top two rows of subplots denoted with .i show the flow-density plane where σ_h increases from the top curve to bottom, while the bottom two rows of subplots denoted with .ii show the exact same data in the speed-flow plane, now σ_h increases from right to left. Throughout, dashed curves are shown for reference across the plots at constant v or u.

lane 5 and (F) all_lanes combined. The top two rows of subplots denoted with .i show the qk plane while the bottom two rows of subplots denoted with .ii show the exact same data in the vq plane.[13] These plots clearly show that the lowest σ_h bin always exhibit the highest flow at the given v (i.e., $\sigma_h < 0.6s$ is the top-most curve in the qk plane and right-most curve in the vq plane) and that the flow at a given speed progressively drops as one moves to the next highest σ_h bin. In other words, **Lanes 1-5 taken individually and all_lanes**

[13] For brevity, the plots show all 7 stations pooled, when taking each station individually the general shape does not change, but noise increases. Two of the data sets (CMFMS and Pinole) only contain a single detector station, which in turn, shows examples of stations taken individually. Also note that it is rare that the all_lanes exhibit $\sigma_h < 0.6s$ using 2 mph bins, so in this data set for all_lanes the lowest σ_h bin only exceeds the threshold of at least 50 observations per bin between 18 and 44 mph.

combined show the same trend: the Q(k) progresses from a triangular shape for the samples with low σ_h to a concave shape from the samples with high σ_h.

Fig. 6 repeats the comparisons only now using the BHL wb 2003 data set and the general trends are unchanged. The one exception is the curve for samples with $\sigma_h > 1.2s$ in lane 1, as shown in Fig. 6A.ii. Like the previous data set, lane 1 is a time of day HOV lane and in this case the highest σ_h bin shows the double peaking due to combining HOV and non-HOV periods that was previously seen in lane 1 Fig. 3. Fig. 7 repeats the comparisons using the CMFMS wb 2008 data set. This site only has three lanes, but they are all general purpose lanes (no HOV). This site sees less congestion so the retention thresholds were reduced for this data set (25 samples per bin instead of 50), as a result, the curves are noisier than the other data sets; but each lane and all_lanes combined continue to show the trend where the Q(k) progresses from a triangular shape when calculated from samples with low σ_h to a concave shape when calculated from samples with high σ_h. Note that because the speed limit is only 55 mph at this site the curves are terminated at lower top speed than the

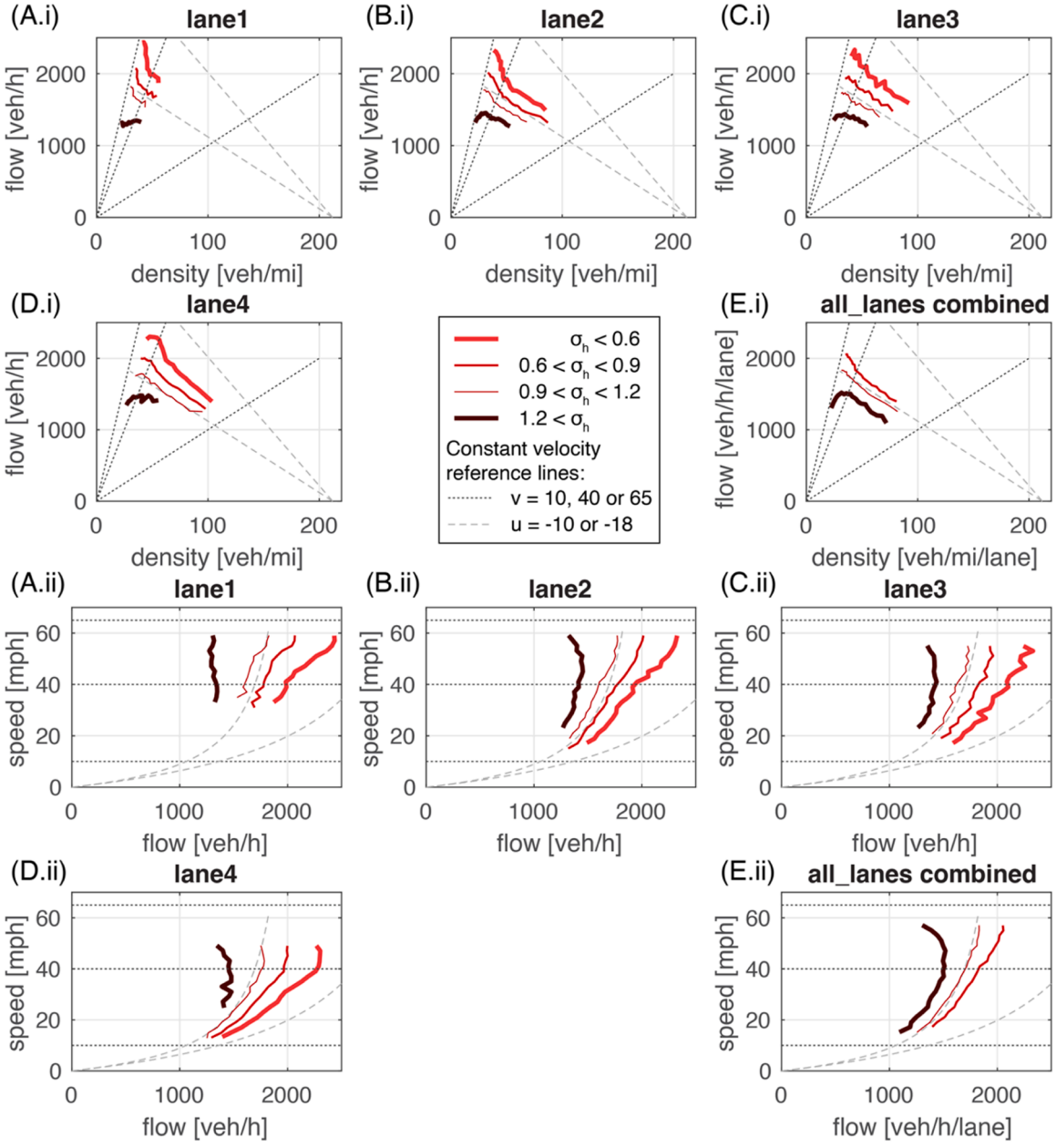

Fig. 8. Curves showing the median EVA (q,k,v) in each speed bin from the Pinole eb 2010 data set for the four different σ_h bins in (A) Lane 1 to (D) lane 4, and (E) all_lanes combined. The top two rows of subplots denoted with .i show the flow-density plane where σ_h increases from the top curve to bottom, while the bottom two rows of subplots denoted with .ii show the exact same data in the speed-flow plane, now σ_h increases from right to left. Throughout, dashed curves are shown for reference across the plots at constant v or u.

other sites. Fig. 8 repeats the comparisons using the Pinole eb 2010 data set, where the speed limit is 65 mph, lane 1 is a time of day HOV lane, and there are only four lanes. Like the CMFMS data, there is only one detector station in this data set. Once more the trends are readily evident. Fig. 9 repeats the comparisons using the FSP sb 1993 data set. The speed limit is 65 mph, lane 1 is a time of day HOV lane, and there are only four lanes. In this case the Q(k) from the samples with $\sigma_h > 1.2s$ in lane 2 still exhibits a triangular shaped Q(k), as shown in Fig. 9B.ii. As will be seen in Fig. 10Q, lane 2 consistently has very high flow, this result arises because this segment is immediately upstream of a lane drop and during the periods of highest demand lane 1 only serves HOV vehicles.

All five of the data sets show the same trend: the Q(k) progresses from a triangular shape when Q(k) is created from samples with low σ_h to a concave shape when Q(k) is created from samples with high σ_h. Recall that collectively, these data sets span over 18 years. Since the data in a given subplot are from the same location and lane, and successive samples will often wind up in different $\sigma_h$bins, **the difference between the high and low σ_h curves is not related to location, traffic patterns or time of day**.

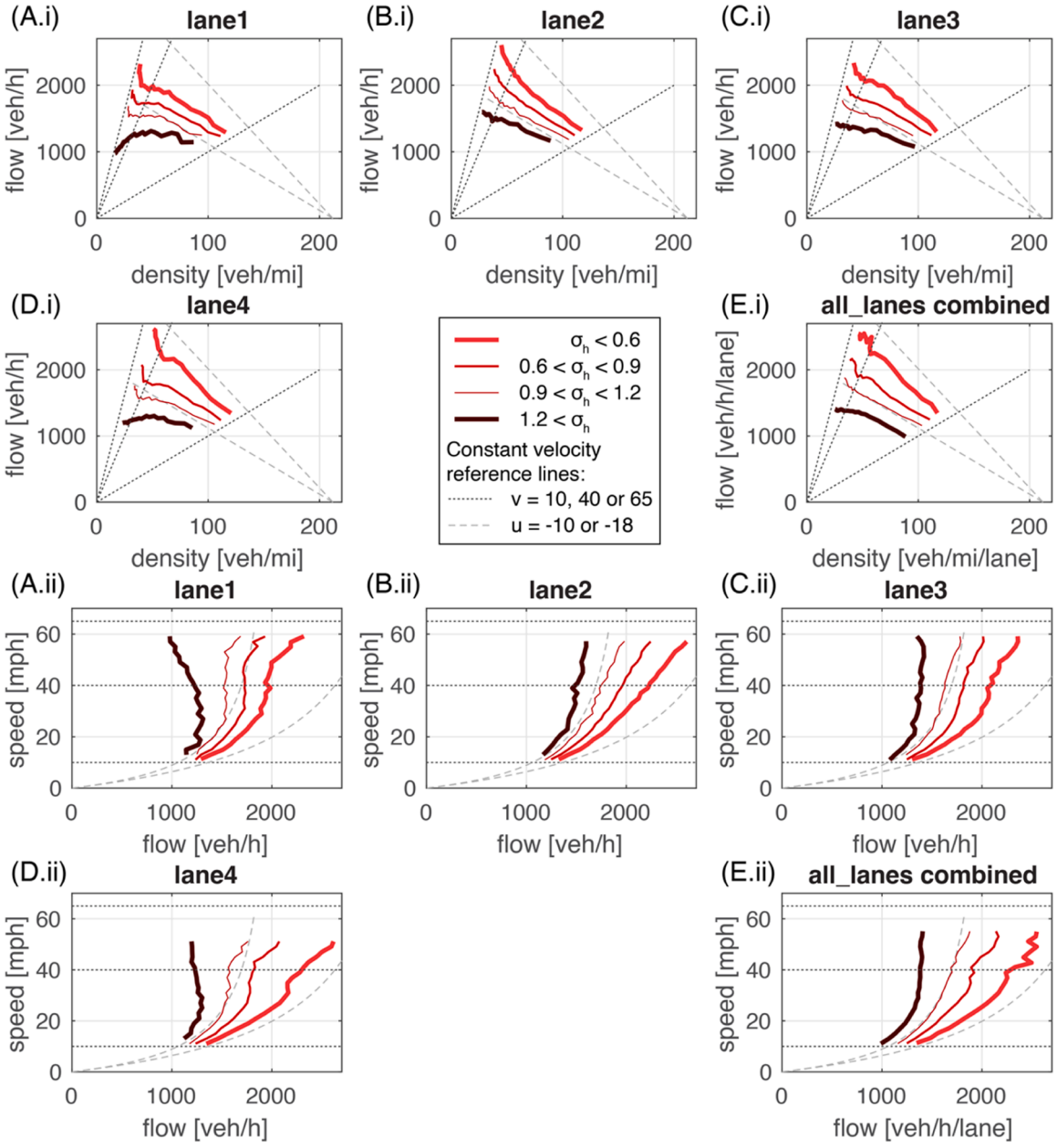

Fig. 9. Curves showing the median EVA (q,k,v) in each speed bin from the FSP sb 1993 data set for the four different σ_h bins in (A) Lane 1 to (D) lane 4, and (E) all_lanes combined. The top two rows of subplots denoted with .i show the flow-density plane where σ_h increases from the top curve to bottom, while the bottom two rows of subplots denoted with .ii show the exact same data in the speed-flow plane, now σ_h increases from right to left. Throughout, dashed curves are shown for reference across the plots at constant v or u.

While the results are shown without the temporal dimension, one should remember that σ_h can change dramatically from one sample to the next, e.g., a LHV might yield a sample with high σ_h while the moving queue behind the LHV could cause the next sample to exhibit a low σ_h. Because σ_h changes like this, the Q(k) can rapidly flicker from one curve to another in Fig. 5-9. It is also interesting to observe that the gaps that pull q down have little impact on the sample speed. As a result, **the non-stationary concave Q(k) falls inside the stationary triangular Q(k)** and the resulting concave shape simply reflects the presence of the microscopic non-stationary transients in the underlying samples used to generate the FD.

3.1.2. From standard deviation of headway to long headway

The first two columns of subplots in Fig. 10 repeat the analysis using all of the data, without binning by σ_h. Thus, Fig. 10A-B repeat

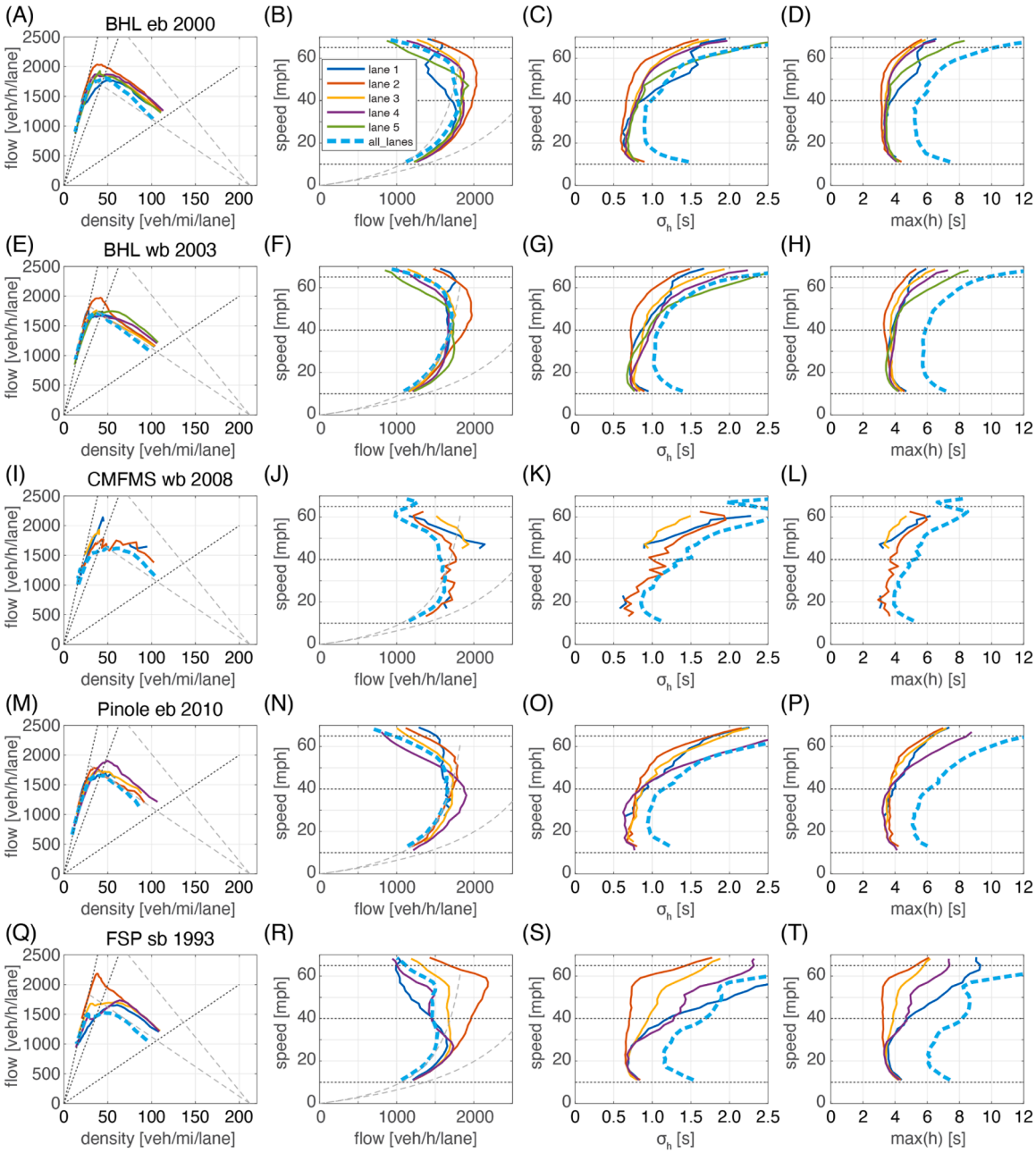

Fig. 10. One row of subplots for each data set. The first column of subplots show the curves of median EVA (q,k,v) in flow-density plane for each speed bin for each lane and all_lanes for the given data set, the second column of subplots repeat these data in speed-flow plane. Throughout, dashed curves are shown for reference across the plots at constant v = 10, 40 and 65 mph, and u = -10 and -18 mph. The third column of subplots show the corresponding curves of median σ_h in a given sample, and the fourth column of subplots show curves of median max(h) in a given sample.

Fig. 3, while each subsequent row of subplots show the corresponding results for the other data sets. One small change is made in the analysis as we move to Fig. 10, now the data are limited to the time period of 6 am to 8 pm because the early morning hours exhibit very low flows.

Every lane in every data set except lane 2 in FSP sb 1993 (Fig. 10Q) and the all_lanes combined condition in all of the data sets exhibit a concave Q(k) when σ_h is ignored. As discussed above, lane 2 in FSP sees high q because it is the fastest general purpose lane immediately upstream of a lane drop bottleneck.

Upon reviewing the first two columns of subplots in Fig. 10, an astute reader might notice that the all_lanes Q(k) tends to fall inside the Q(k) from the individual lanes in the given data set. At first this outcome might seem counter-intuitive, but it should be expected. Consider the hypothetical scenario where a single static concave FD applies to every lane individually. It is rare that all lanes will exhibit the same speed in a given sample period. If different lanes take different speeds on the same concave FD, the average across the different lanes must fall inside the single lane concave FD because of the concavity of the curve. In fact, the rules of the road dictate that traffic should sort itself with faster vehicles on the inside lane, leading to standing speed gradients between lanes, while imbalanced demand during congestion can lead to even more extreme standing speed gradients between lanes. The situation is further compounded at locations with an HOV lane because the HOV lane is often freely flowing while the other lanes are congested. When at least one lane is free flowng and at least one other lane is congested like this, the resulting all_lanes state should fall inside the true FD, independent of whether the FD is concave or triangular.

Looking at these data from another perspective, the third column of subplots in Fig. 10 shows that the corresponding median σ_h for each speed bin increases with speed for v>20 mph. It is often assumed that when traffic exhibits a concave Q(k) like this, that the individual vehicles underlying the sample are roughly homogeneous, or "near stationary." But the last column of subplots show the median of the maximum headway, max(h), seen in the given sample for the given speed bin, and like σ_h, the max(h) generally increases with speed for v>20 mph. Taking the data from these last two columns of subplots, Fig. 11 plots max(h) versus σ_h for each lane and all_lanes combined for each of the five data sets. In all cases a roughly linear relationship emerges. Returning to the raw EVA measurements for each sample: q, k, v, σ_h, and max(h), for each lane and all_lanes combined at each station we did a first order linear regression of max(h) to σ_h. The resulting parameters are shown in Table 2. There is a strong correlation between max(h) and σ_h, in every single case the correlation coefficient is at least 0.91 (median value of 0.97). Across the individual lanes the minimum R^2 for the linear fit was 0.92 (median value 0.95) while dipping as low as 0.82 for all_lanes combined. Applying the fitted model to the threshold of the longest σ_h bin, $\sigma_h = 1.2s$, the smallest estimate of max(h) across all of the fittings is 4.0 sec (median value of 4.6 sec). In short, **max(h) increases roughly linearly with σ_h, thus, as σ_h increases not only does Q(k) become more concave, but the expected longest headway in a given sample also grows, i.e., the microscopic voids from LHV that are too small to be perceptible in the conventional detector data are large enough to disrupt assumptions of homogeneity and stationarity within the given sample.** The last column of subplots in Fig. 10 reaffirms this outcome, the median of max(h) in individual lanes steadily increases from about 4 sec at 40 mph to about 6 sec at 60 mph.

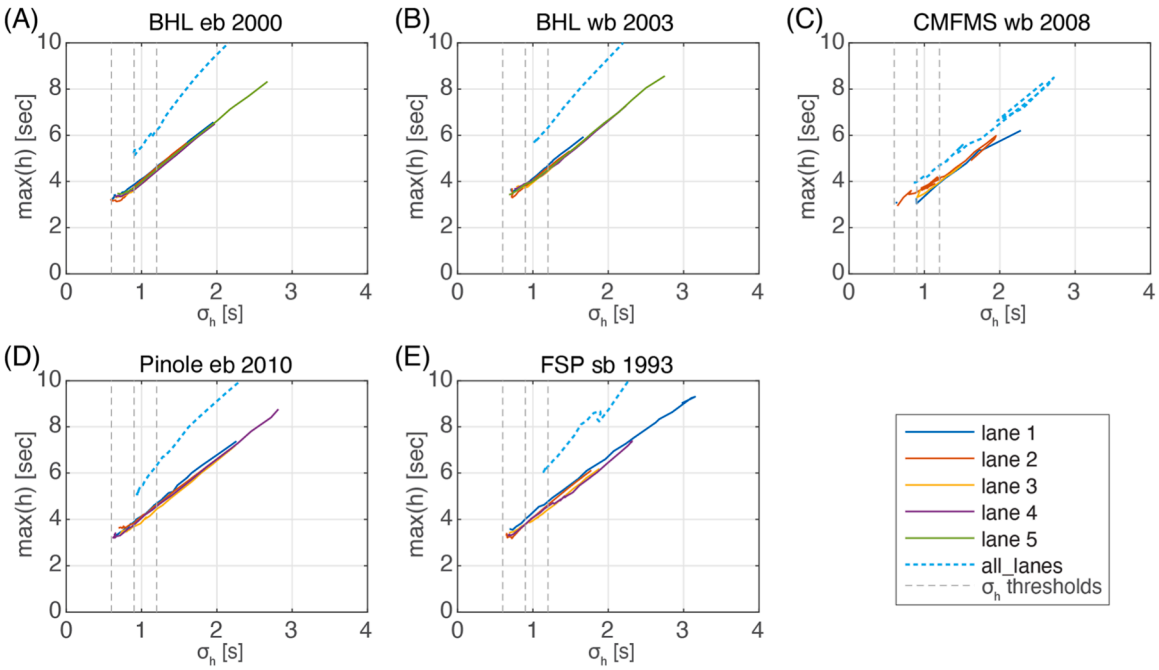

Fig. 11. max(h) versus σ_h for each speed bin in the given lane or all_lanes in the given data set for (a) BHL eb 2000, (B) BHL wb 2003, (C) CMFMS wb 2008, (D) Pinole eb 2010, and (E) FSP sb 1993. Note that the curves for the individual lanes generally fall on top of one another, making it difficult to distinguish the different curves. This similarity across lanes is a key feature that the plots seek to present. Throughout dashed lines are shown at the σ_h thresholds between successive σ_h bins.

Table 2
Results of a first order linear regression of max(h) to σ_h by individual lane and separately all_lanes combined for each station.

data set	lane	intercept	slope	R^2	Correlation coefficient	# samples used
BHL eb 2000	1	1.59	2.47	0.96	0.98	134,415
	2	1.49	2.59	0.94	0.97	296,092
	3	1.42	2.56	0.94	0.97	264,125
	4	1.41	2.56	0.93	0.97	256,630
	5	1.52	2.54	0.95	0.97	219,866
	all_lanes	1.85	3.89	0.82	0.91	310,854
BHL wb 2003	1	1.68	2.52	0.95	0.98	275,943
	2	1.59	2.61	0.92	0.96	257,220
	3	1.61	2.52	0.93	0.96	264,451
	4	1.57	2.53	0.94	0.97	263,877
	5	1.57	2.53	0.95	0.98	268,266
	all_lanes	1.86	3.89	0.84	0.92	344,050
CMFMS wb 2008	1	1.25	2.33	0.97	0.99	4,228
	2	1.26	2.40	0.96	0.98	16,409
	3	1.11	2.40	0.97	0.99	6,854
	all_lanes	1.35	2.58	0.94	0.97	76,825
Pinole eb 2010	1	1.64	2.52	0.95	0.98	91,892
	2	1.56	2.53	0.95	0.97	130,197
	3	1.44	2.51	0.95	0.98	66,971
	4	1.55	2.51	0.95	0.98	99,464
	all_lanes	2.80	3.09	0.84	0.92	144,715
FSP sb 1993	1	1.77	2.41	0.96	0.98	117,955
	2	1.47	2.64	0.94	0.97	261,346
	3	1.48	2.53	0.94	0.97	263,930
	4	1.53	2.46	0.96	0.98	161,357
	all_lanes	0.93	4.14	0.88	0.94	301,166

3.2. The sixth data set- the earliest empirical FD's

Section 1.2 argued that short-duration disturbances like a void ahead of LHV are large enough to disrupt stationarity but these disturbances are too short to be perceptible at the resolution of conventional data aggregation. Section 3.1 then demonstrated that indeed, as σ_h increases, the largest void in the sample increased (over 4 sec for $\sigma_h > 1.2s$) while the shape of Q(k) progressed towards concave shape. As per Fig. 1, a Q(k) constructed from non-stationary samples can yield a reproducible concave Q(k) that mimic the appearance of a stationary concave FD. Or to put it another way, based strictly on the shape of Q(k) one cannot ascertain whether the curve is derived from stationary conditions or from non-stationary conditions.

With this view in mind, let us now consider the seminal concave FD from Greenshields (1935) that inspired LWR. We will call this curve G35. Greenshields's study sought to establish the functional capacity of a "two-lane highway," i.e., two way traffic with one lane in each direction. Greenshields ultimately used seven independent observation periods to measure q and v, from which k was then calculated. The result is a single measurement of the average traffic state for each of the seven samples. Each of the six free flow data points included at least 160 vehicles (mean size 412 vehicles) observed over a sample period of at least 6 min (mean duration 22.7 min). Greenshields (1935) only presents a small example of the individual vehicle measurements, but from the 35 successive vehicles shown in the paper, half of the headways are greater than 10 sec while the individual vehicle speeds ranged between 20 and 62 mph (median 46 mph). Separately, the paper provides a distribution of speeds for a few of the samples, in each case the quartiles fall near 28 and 48 mph, corresponding to a factor of 1.7 across the interquartile range. Given the large range of speeds, large headways are to be expected as fast vehicles pull away from slow vehicles behind and in turn, the slow vehicles collect many vehicles behind as the drivers wait for an opportunity to overtake; thus, giving rise to a succession of moving bottlenecks with voids ahead and moving queues behind. Notably, overtaking on a two-lane highway requires a very large void in the oncoming traffic. Consistent with the $\sigma_h > 1.2s$ Q(k) from EVA applied to loop detector data, **the traffic underlying each sample in G35 is non-stationary even though the concave Q(k) is smooth and yields a good fit to the empirical data**.

It turns out G35 is not the first recorded FD, Greenshields (1934) undertook a related study, this time, to effectively find q as a function of v. Research starting in the early 1920's sought to establish a theoretical speed-flow relationship of a single lane (Johnson, 1921; Johnson 1926; Hamlin, 1928; Johnson, 1929, Dougherty, 1930, 1931; and Johannesson, 1931). Unlike the preceding studies, Greenshields (1934) appears to be the first FD study that sought to fit empirical data rather than starting with some assumed functional form. Recognizing that it is rare to find long queues moving at constant speed, Greenshields (1934) studied small platoons of vehicles trapped behind slow moving vehicles on two-lane highways. Specifically, Greenshields used a high speed camera to measure the speed and spacing of 794 individual vehicles caught in moving queues, sorted these measurements into 2 mph bins, calculated the average spacing in each of the bins, and then fit a straight line to these averages. In this way, he measured a speed-spacing curve that he then projected into the speed-flow plane. We will call this curve G34, and because it strictly consists of vehicles caught inside moving queues, the sample in each bin was from homogeneous traffic. Reiterating the key figures from Greenshields (1934), Fig. 12A shows his speed-spacing curve and Fig. 12B projects his curve into the speed-flow plane and he shows the curves from several of the preceding models for reference.

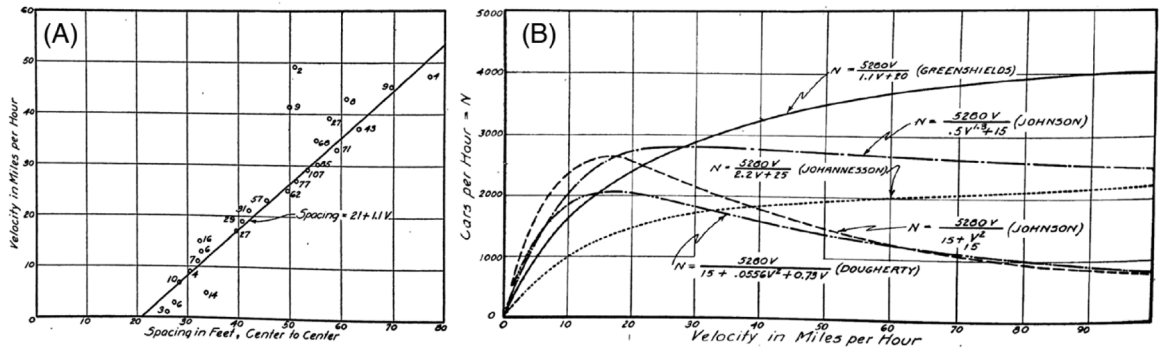

Fig. 12. Figures from Greenshields (1934) showing (A) his linear speed spacing data and curve fit, (B) several speed-spacing models of the day projected into the speed-flow plane.

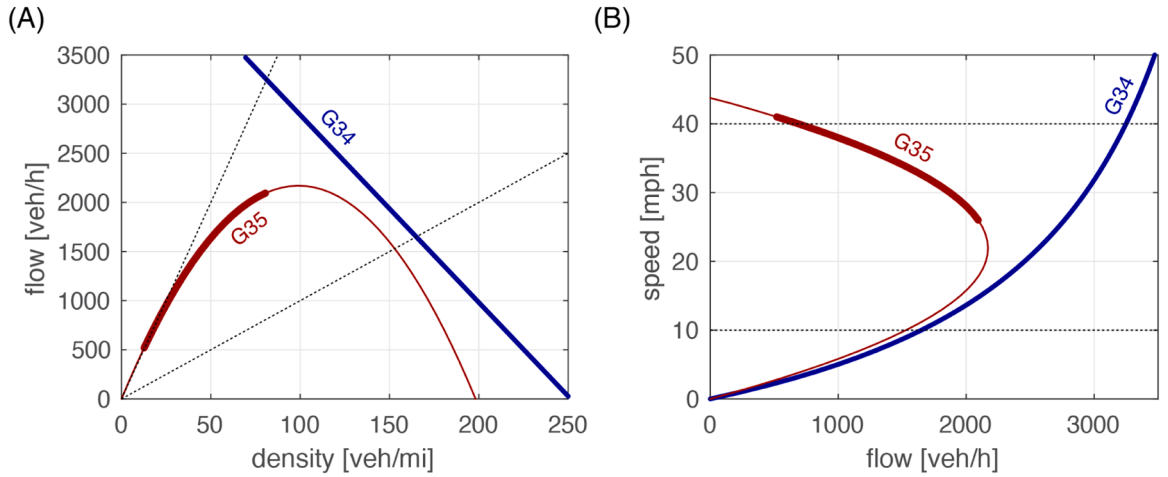

Fig. 13. The two models from Greenshields (A) in the flow-density plane, and (B) the speed-flow plane. Both curves are plotted with a bold line over the range of states Greenshields used for fitting the data: G34: $v \leq 50$ mph, and G35: $v > 25$ mph & $q > 400$ vph. Dashed lines at 10 mph and 40 mph added for reference.

The final models from the respective papers give G34 in Equation 20 and G35 in Equation 21 (in both equations v is in mph and k in veh/mi). Fig. 13 projects the resulting curves into the flow-density plane and separately into the speed-flow plane. The triangular G34 arises from homogeneous (and thus, stationary) samples of congested vehicles and is very similar in form to the low σ_h from the loop detectors. Meanwhile, the concave G35 arises from non-stationary samples of whatever vehicles happened to pass during the observation period and is even more concave than the highest σ_h from the loop detectors. In this way, **the very first empirical FD provide historical evidence to support our findings that samples of stationary traffic tend towards a triangular Q(k) while samples of non-stationary traffic tend toward a concave Q(k) with lower max q,** thereby adding an element of timelessness to the present work.

$$\text{G34}: \; k = \frac{5280}{21 + 1.1 \cdot v} \tag{20}$$

$$\text{G35}: \; k = \frac{43.8 - v}{0.221} \tag{21}$$

4. Conclusions

This paper studied microscopic voids in the traffic stream that are too small to be perceptible in conventional detector data but are large enough to disrupt some of the assumptions used in HdTFM. This work used loop detector data sets collected at five different sites, collected over a span of more than 18 years. The very first empirical FD provide historical evidence to support the loop detector findings and adds an element of timelessness to the present work and collectively, the results span over 75 years of empirical traffic data. There are six main conclusions that arise from this analysis. Each one addressed in its own subsection below. The notation in this section uses Q(k) to denote the calculated curve, separate from the theoretical concept of a FD.

4.1. The shape of equilibrium FD appears to be triangular

This work has shown that the emergent Q(k) progresses from a triangular shape when Q(k) is created from samples with low σ_h to a concave shape that falls inside the triangular curve when Q(k) is created from samples with high σ_h. Furthermore, as σ_h increases not only does Q(k) become more concave, but the expected longest headway in a given sample also grows, i.e., the microscopic voids from LHV that are too small to be perceptible in the macroscopic data are large enough to disrupt stationarity within the given sample.

As noted earlier, these voids ahead of the LHV are inherently non-stationary because different regions of the sample are perceptively distinct. As discussed in Section 4.2, the sub-sample disturbances can have significant impact at the macroscopic scale if they contain unobserved boundary conditions. Zhang (1999) argued that traffic is only in equilibrium when the temporal stationary condition of Equation 22 holds and in non-equilibrium otherwise. At the successive vehicle level, if $\frac{\partial v}{\partial t} \neq 0$, the sample is non-equilibrium by definition and if $\frac{\partial v}{\partial t} = 0$, then the LHV correspond to transient low k in the sample, i.e., $\frac{\partial k}{\partial t} \neq 0$, and again, the sample is non-equilibrium. Thus, by these measures only the low σ_h curves could be equilibrium FD curves. In other words, these results indicate that **if the equilibrium FD curve was observed, then for all six data sets it is the triangular shape from low σ_h.**

$$\frac{\partial v}{\partial t} = 0; \frac{\partial k}{\partial t} = 0 \tag{22}$$

This point is readily apparent in Greenshields two curves (Fig. 13). G35 was sampled under extremely inhomogeneous (non-stationary, non-equilibrium) conditions and gives rise to a concave Q(k). Whereas, G34 came from the same class of roadway, but in this case, Greenshields was careful to ensure homogeneous conditions, and the resulting Q(k) is triangular in shape.

This work did not evaluate $\frac{\partial v}{\partial t}$ and Zhang (1999) also postulated strong criteria for equilibrium that considers the partial derivatives in space, which cannot be tested directly with the dual loop detector data. So, it is possible that none of the observed curves represent an equilibrium FD curve under Zhang's criteria. But it is safe to say that **the concave Q(k) seen throughout this study do not represent the equilibrium FD under Zhang's criteria**.

4.2. Conventional detector data mask critical features needed by HdTFM

On the one hand, just because HdTFM are macroscopic models, it does not mean that the models will always work well with conventional fixed time averaged data (Section 2.1). Consider a hypothetical example where a queue backs up past a detector station. For ease of illustration suppose the state transitions instantaneously and there are only two states observed at this location, corresponding to (A) the free flow conditions before the queue arrives and (B) the congested conditions after. Even if both states are stable, long lasting, and stationary, the fixed time average that spans the arrival of the queue will be non-stationary, containing a portion of time from state A and the rest of time from state B. That fixed time average is meaningless to HdTFM because the average is across two distinct states. In fact, because that sample averages free flow and congested conditions one would expect it to fall somewhere inside the FD, without any significant meaning. This problem arises due to the sampling resolution, in this case the sample boundaries did not align well with the state boundary. This type of blurring should be expected in fixed time averaged data whenever a transition passes.

On the other hand, just because HdTFM are macroscopic models, it does not mean that all features of interest are long lasting. Significant macroscopic features can be too small to be perceived from fixed time averaged data. At best, fixed time averaging can only resolve dynamics that last as long as the sample period. But realistically, dynamics would likely have to last several samples to be perceptible. This work found evidence of extremely short duration dynamics far below the resolution of fixed time sampling that (i) impact the emergent Q(k) as per Section 4.1, and (ii) if they pass undetected can violate the assumptions of HdTFM, as follows.

While the voids from LHV are large enough to impact traffic dynamics (see, e.g., Coifman et al., 2023), their durations are much shorter than conventional sampling periods, thus, their presence cannot be detected in conventional fixed time sampling. From the KW perspective, an undetected void creates an ill posed problem where the traffic state over all time and space is no longer defined strictly by the known boundary conditions. If a driver acts independent of their leader there are no KW from the boundaries that reach the driver during their independence, and thus, there is no way to predict how the driver should act. Instead, the independent LHV driver forms a new independent boundary that emanates unaccounted KW from within the region of interest.

Generally, this problem could be handled by HdTFM if the boundary condition from the LHV were detected, but because of the resolution limitations such detection cannot be achieved with conventional fixed time averaged traffic data. Section 4.5 shows several examples of such events as seen in vehicle trajectory data. It is likely that there are other significant traffic dynamics impacting HdTFM that also go unobserved in fixed time averaged data because the duration of the event is on the order of the sample period or shorter.

4.3. An empirical case study supporting multi-class HdTFM with mixed regime samples

The empirical results in this study underscore the need for multi-class HdTFM. Assuming all significant features are observable (i.e., without any detection limitations as per Section 4.2), following conventional practice of a single Q(k) then SwA and LWR cannot capture the dynamics underlying the mix of LHV and SHV seen in this study. Many single-class higher order models would also be challenged under these conditions. When the emergent state falls in the free flow regime of a concave Q(k), a HdTFM would have to capture the mixed regimes of the quasi-free flowing LHV and queued SHV in a given sample (or more generally, a given region of time and space). Multi-class models are well structured to handle these potentially complex interactions.

For example, Zhang (2002) considered the scenario with non-equilibrium states that could be sustained indefinitely. Zhang's work

effectively replicated the acceleration cycle hysteresis in the FD from Newell (1962) and illustrated the case in which conditions on the coupled FD curves were strictly congested. In this context, one could view the jump from LHV to SHV behind as a contact discontinuity, but unlike Zhang's example, the LHV is operating in the free flow regime of its class-FD while the SHV are operating in the congested regime of their class-FD. Inspired by Daganzo (2002), several multi-class models explicitly consider such mixed regime conditions, e.g., Logghe and Immers (2008).

4.4. An empirical case study illustrating challenges to the predictive abilities of HdTFM

Given sufficient resolution (i.e., without any detection limitations as per Section 4.2), a well-crafted multi-class HdTFM should be able to capture all of the dynamics explored in this paper, but it can only do so a posteriori. A pure HdTFM is deterministic, but the formation and dissolution of the LHV that can create a new boundary condition are random events that cannot be predicted ahead of time. For example, while Zhang (2002) can be used to model the long lasting LHV/SHV interactions observed in Coifman et al. (2023), that model cannot predict the occurrence of any given LHV. This case of significant microscopic disturbances is similar to the long standing issue of stop wave formation and other random events in the HdTFM literature. One could argue that in many cases the microscopic disturbances are trivial and can be ignored. Sometimes the LHV events are short lived, e.g., closing the gap behind a vehicle that exited, but microscopic disturbances can also be long lived, Coifman et al. (2023) studied situations where the LHV persisted for 2/3 mi or further. The longer a LHV persists and the more it deviates from its leader, the more significant it becomes. This issue of *driver agency* is discussed further in Section 4.5.

A few other challenges should be noted. While much of this paper discusses LHV and SHV as if they were homogeneous classes, in reality they reflect a continuum of behavior. Furthermore, the distinction between LHV and SHV is not intrinsic to the given vehicle, and it is only a "tendency" of the driver. Conceptually, the LHV could attenuate or otherwise distort some characteristics rather than always blocking them. LHV could arise for intrinsic reasons, e.g., a driver might prefer a lower free speed or a longer spacing, or extrinsic reasons, e.g., in response to the adjacent lanes, lane change maneuvers, or a driver proactively anticipating an imminent slowdown. So accurately capturing this continuum of behaviors could be difficult with a small number of classes. In spite of these stochastic challenges, while it is impossible to accurately forecast individual random events, it is plausible that a model might be developed that could account for the collective impacts of the stochastic events given their rate of occurrence.

4.5. Driver agency

Some drivers exhibit agency, namely, the gaps ahead of the LHV are at the driver's discretion. As noted in Section 4.2, when the LHV drivers act independent of their leader, these vehicles can both block KW and define a new independent boundary that emanates KW. Presumably the LHV are only semi-independent of their leader e.g., if their leader undertakes a large deceleration the LHV must also slow, but the LHV driver could either close the gap or they could still maintain a large headway when they slow down. In short, the

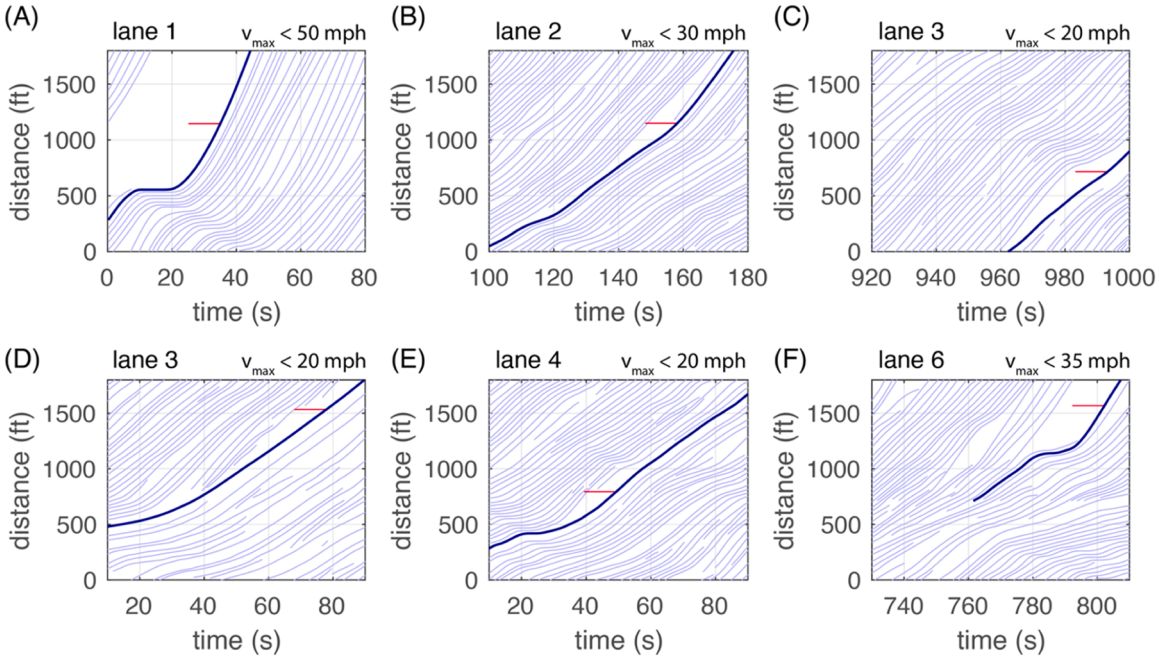

Fig. 14. Six examples of vehicles exhibiting driver agency, as highlighted by the dark trajectory in each plot. In all cases the lane and the subject vehicle's max speed are shown above the plot. These data come from the 17 min long reextracted NGSIM I-80 data set.

LHV drivers are exhibiting driver agency when they choose to take a larger spacing than necessary, and in the process, they violate the conventional assumptions, "that vehicles capture no more space than strictly necessary" (Logghe and Immers, 2008). If the drivers were self-consistent, new classes could be created and these unusual drivers could be accommodated with multi-class models.

But driver agency also applies to sustaining and dissolving a long headway. Driver agency leads to the uncertainty of the stochastic LHV events that challenge the predictive ability of a deterministic HdTFM. A single driver can abruptly change their behavior in a way that literally has wide ranging impacts: The driver could maintain the gap resulting in signals moving downstream with their vehicle (e.g., Fig. 1B) at the risk of attracting another vehicle to enter the lane in the gap (more uncertainty), or the driver could close the gap resulting in upstream moving signals (e.g., Fig. 1C) while choosing to do so either quickly or slowly (further uncertainty). Yet these behavioral changes would be difficult or impossible to anticipate.

Driver agency is difficult to illustrate using loop detector data that only capture the vehicle at a single point in time and space. Clear examples of driver agency can be seen in all six lanes of the reextracted NGSIM I-80 data set (Coifman and Li, 2024). Conditions throughout this data set are well into the congested regime (except for lane 1 which is a HOV lane). The dark trajectories in Fig. 14 show six examples of vehicles that maintained a long headway for at least 20 sec, and during that period the headway exceeded 8 sec at least once. For reference, a 10 sec long horizontal red line is shown in each subplot near the location where the given vehicle exhibited its largest headway. All these examples were inspected in the validation video. Parts A and F show an unwilling car caught behind another vehicle that ignored downstream conditions in the ego lane when they slowed or stopped to match the speed in an adjacent lane as they changed lanes. Part B shows a pickup truck that simply chose to move slower than its leader and parts C-E show semi-trailer trucks that apparently chose more conservative acceleration than the other vehicles (not all semi-trailer trucks exhibited this behavior). In the case of part C, the truck driver appears to have anticipated the forthcoming slow wave. Sometimes the voids ahead of the LHV are partially filled by entering vehicles (parts B, D & E) sometimes the driver closes the gap without any entrances ahead (part C) or the gap simply persists unfilled when it exits the link (parts A & F).

4.6. A test for stationary conditions when you need it

The application of any hydrodynamic or continuum traffic flow model needs to be cognizant of the underlying microscopic processes that enable the assumed macroscopic dynamics. As shown herein, there can be microscopic processes far below the detector's sampling resolution that yield a reproducible concave FD but also violate the presumed stationarity. Whenever a model relies on the shape of the FD to determine the velocities at which signals and characteristics propagate through the traffic stream, one must be mindful of the microscopic dynamics that are necessary to give rise to a macroscopic model and be careful to investigate a concave FD to ensure it supports the assumptions placed upon it. To this end, if the individual vehicle actuations are available, the EVA method binned by σ_h developed in this paper offers a simple test of stationary conditions.

Author statement

as per: https://www.elsevier.com/authors/journal-authors/policies-and-ethics/credit-author-statement

Benjamin Coifman: Conceptualization, Methodology, Software, Formal analysis, Investigation, Writing, Visualization, Funding acquisition

CRediT authorship contribution statement

Benjamin Coifman: Writing – review & editing, Writing – original draft, Visualization, Validation, Methodology, Investigation, Funding acquisition, Formal analysis, Data curation, Conceptualization.

Acknowledgements

This material is based in part upon work supported in part by the National Science Foundation under Grant No. 1537423 and 2023857. The contents of this report reflect the views of the authors who are responsible for the facts and the accuracy of the data presented herein. This report does not constitute a standard, specification or regulation.

Appendix A

This section presents some of the finer details of dual loop detector measurements, it is not critical to understanding the rest of the paper, but these subtle details are very important for anyone who wishes to reproduce or extend this work. The individual vehicle actuations used in this work are rarely recorded by operating agencies, typically they are aggregated in the field for FTS and then the individual vehicle actuations are discarded. So simply getting the individual vehicle actuations can be a logistical challenge. One should not expect consistency between operating agencies in the way detector measurements are calculated, in fact sometimes a given agency might calculate the measurements differently at different detector stations. Meanwhile, the quality of the detector data depends on how well the detectors were tuned in the field. Although many tuning and calibration errors cannot be corrected post hoc, a few can be (Lang and Coifman, 2006; Lee and Coifman, 2012b) while the presence of other chronic errors can be identified (Coifman, 1999; Lee and Coifman, 2011 & 2012a). Obviously, the best strategy is to work with the operating agency to ensure the detectors are well tuned prior to data collection, but that is not always feasible.

A vehicle passing over a dual loop detector should register four events: upstream detector rising and falling transitions and downstream rising and falling transitions. Where a rising transition is when the given detector is first occupied by the vehicle and a falling transition is when the vehicle clears the detector. From these four events it is straight forward to measure the traversal time from either the paired rising transitions or paired falling transitions; and the on-time from the difference between the falling and rising transition times at either of the detectors. The two pairs of measurements could be combined or averaged in many different ways, and in fact the four transitions themselves can be aggregated in more complex ways (Wu and Coifman, 2014). It should be expected that a small percentage of vehicles will only be detected by just one of the paired loop detectors either due to a lane change maneuver or a detector error. For the EVA method we exclude any unmatched actuation seen at just one of the dual loop detectors and then exclude the following vehicle from the EVA calculations because its true headway is unknown.

For greatest fidelity, in this paper we use the paired rising transitions to measure speed because the rising transition is more consistent across vehicles than the falling transition (Lee and Coifman, 2011) since the distribution of metal tends to be greater and closer to the ground in the front of most vehicles. Generally, the period of time that speed and on-times are measured will not align perfectly, in which case vehicle acceleration might cause discrepancies between the speed and on-time measurements. To minimize these impacts, the upstream on-time measurement has the greater overlap with the period that speed is measured via the rising transitions (Wu and Coifman, 2014), so we use upstream on-time to go with the choice of measuring speed from the paired rising edges. Meanwhile, one could define the vehicle's arrival time to be anything between the upstream rising edge and downstream falling edge transition, what is important is that the choice is consistent across all vehicles. We arbitrarily choose the upstream detector's rising edge transition time for the vehicle arrival time.

References

Benzoni-Gavage, S., Colombo, R., 2003. An n-Populations Model for Traffic Flow. European Journal of Applied Mathematics 14 (5), 587–612.
Cassidy, M., 1998. Bivariate Relations in Nearly Stationary Highway Traffic. Transportation Research Part B 32 (1), 49–59.
Chanut, S., Buisson, C., 2003. Macroscopic Model and its Numerical Solution for Two-Flow Mixed Traffic with Different Speeds and Lengths. Transportation Research Record 1852 (1), 209–219.
Chen, D., Ahn, S., 2018. Capacity-Drop at Extended Bottlenecks: Merge, Diverge, and Weave. Transportation Research Part B: Methodological 108, 1–20.
Coifman, B., 1999. Using Dual Loop Speed Traps to Identify Detector Errors. Transportation Research Record (1683), 47–58.
Coifman, B., 2001. Improved Velocity Estimation Using Single Loop Detectors. Transportation Research: Part A 35 (10), 863–880.
Coifman, B., 2014a. Jam Occupancy and Other Lingering Problems with Empirical Fundamental Relationships. Transportation Research Record 2422, 104–112.
Coifman, B., 2014b. Revisiting the Empirical Fundamental Relationship. Transportation Research- Part B 68, 173–184.
Coifman, B., 2015. Empirical Flow-Density and Speed-Spacing Relationships: Evidence of Vehicle Length Dependency. Transportation Research- Part B 78, 54–65.
Coifman, B. (2024). Data Sets, https://u.osu.edu/coifman.1/data-sets/.
Coifman, B., Kim, S., 2011. Extended Bottlenecks, the Fundamental Relationship, and Capacity Drop on Freeways. Transportation Research- Part A 45 (9), 980–991.
Coifman, B., Li, L., 2024. Partial Trajectory Method to Align and Validate Successive Video Cameras for Vehicle Tracking. Transportation Research Part C 158.
Coifman, B., Lyddy, D., Skabardonis, A., 2000. The Berkeley Highway Laboratory- Building on the I-880 Field Experiment. In: Proc. IEEE ITS Council Annual Meeting. IEEE, pp. 5–10.
Coifman, B., Neelisetty, S., 2014. Improved Speed Estimation from Single Loop Detectors with High Truck Flow. Journal of Intelligent Transportation Systems 18 (2), 138–148.
Coifman, B., Ponnu, B., 2020. Adjacent Lane Dependencies Modulating Wave Velocity on Congested Freeways- An Empirical Study. Transportation Research Part B 142, 84–99.
Coifman, B., Ponnu, B., El Asmar, P., 2023. LWR and Shockwave Analysis- Failures Under a Parabolic Fundamental Relationship and Unexpected Induced Disturbances. Transportation Research Part A 175.
Daganzo, C., 2002. A Behavioral Theory of Multi-Lane Traffic Flow. Part I: Long Homogeneous Freeway Sections. Transportation Research Part B: Methodological 36 (2), 131–158.
Del Castillo, J., Benitez, F., 1995. On the Functional Form of the Speed-Density Relationship—I: General Theory. Transportation Research Part B: Methodological 29 (5), 373–389.
Dougherty, N., 1930. A Discussion of Road Capacity. Roads and Streets 70 (9), 319–321.
Dougherty, N., 1931. Traffic Capacity of Highways. Seventeenth Annual Road School 42–48.
Drake, J., Schofer, J., May, A., 1967. A Statistical Analysis of Speed Density Hypotheses, *Highway Research Record* (154), 53–87.
Duret, A., Bouffier, J., Buisson, C., 2010. Onset of congestion from low-Speed Merging Maneuvers Within Free-Flow Traffic Stream: Analytical Solution. Transportation Research Record 2188 (1), 96–107.
Edie, L., Baverez, E., 1967. Generation and Propagation of Stop-Start Traffic Waves. In: Proceedings of the Third International Symposium on the Theory of Traffic Flow. Operations Research Society of America.
Greenshields, B., 1934. The Photographic Method of Studying Traffic Behavior. Highway Research Board Proceedings 13 (1), 382–399.
Greenshields, B., 1935. A Study of Traffic Capacity. Proc. of the Highway Research Board 14, 448–477.
Hall, F., Allen, B., Gunter, M., 1986. Empirical Analysis of Freeway Flow-Density Relationships. Transportation Research Part A: Policy and Practice 20 (3), 197–210.
Hamlin, G., 1928. Report of Committee on Highway Traffic Analysis. Highway Research Board Proceedings 7 (1), 229–247.
Johannesson, S., 1931. Highway Economics. McGraw-Hill.
Johnson, A.N., 1921. Traffic Study Proves Two Lane Road Widths Sufficient. Engineering News-Record 86 (23), 989–991.
Johnson, A.N., 1926. Elements Governing the Development of Highway Traffic. Transactions of the American Society of Engineers 89 (1), 259–267.
Johnson, A.N., 1929. Maryland Aerial Survey of Highway Traffic Between Baltimore and Washington. Highway Research Board Proceedings 8 (1), 106–115.
Lang, L., Coifman, B., 2006. Identifying Lane Mapping Errors at Freeway Detector Stations. Transportation Research Record 1945 89–99.
Laval, J., 2009. Effects of geometric design on freeway capacity: Impacts of Truck Lane Restrictions. Transportation Research Part B: Methodological 43 (6), 720–728.
Leclercq, L., Chanut, S., Lesort, J.B., 2004. Moving Bottlenecks in Lighthill-Whitham-Richards Model: A Unified Theory. Transportation Research Record 1883 (1), 3–13.
Leclercq, L., Knoop, V., Marczak, F., Hoogendoorn, S.P., 2016. Capacity Drops at Merges: New Analytical Investigations. Transportation Research Part C: Emerging Technologies 62, 171–181.
Lee, H., Coifman, B., 2011. Identifying and Correcting Pulse-Breakup Errors from Freeway Loop Detectors. Transportation Research Record 2256, 68–78.
Lee, H., Coifman, B., 2012a. Identifying Chronic Splashover Errors at Freeway Loop Detectors. Transportation Research-Part C 24, 141–156.

Lee, H., Coifman, B., 2012b. Quantifying Loop Detector Sensitivity and Correcting Detection Problems on Freeways. ASCE Journal of Transportation Engineering 138 (7), 871–881.
Li, J., Zhang, H., 2011. Fundamental Diagram of Traffic Flow: New Identification Scheme and Further Evidence from Empirical Data. Transportation Research Record 2260, 50–59.
Lighthill, M., Whitham, G., 1955. On Kinematic Waves II. a Theory of Traffic Flow on Long Crowded Roads. Proc. Royal Society of London, Part A 229 (1178), 317–345.
van Lint, J.W.C., Hoogendoorn, S., Schreuder, M., 2008. Fastlane: New Multiclass First-Order Traffic Flow Model. Transportation Research Record 2088 (1), 177–187.
Logghe, S., Immers, L., 2003. Heterogeneous Traffic Flow Modelling with the LWR Model Using Passenger-Car Equivalents. In: Proceedings of the 10th World Congress on ITS. Madrid (Spain), pp. 1–15.
Logghe, S., Immers, L., 2008. Multi-Class Kinematic Wave Theory of Traffic Flow. Transportation Research Part B: Methodological 42 (6), 523–541.
Munjal, P., Hsu, Y., Lawrence, R., 1971. Analysis and Validation of Lane-Drop Effects on Multi-Lane Freeways. Transportation Research 5 (4), 257–266.
Munoz, J., Daganzo, C., 2002. Moving Bottlenecks: A Theory Grounded on Experimental Observation. In: Proc. of the 15th International Symposium on Transportation and Traffic Theory (ISTTT15), pp. 441–461.
Newell, G., 1962. Theories of instability in dense highway traffic. J. Operations Research Society of Japan 5 (1), 9–54.
Newell, G., 1998. A Moving Bottleneck. Transportation Research Part B: Methodological 32 (8), 531–537.
Newell, G., 2002. A simplified car-following theory: a lower order model. Transportation Research Part B 36, 195–205.
Ngoduy, D., Liu, R., 2007. Multiclass First-Order Simulation Model to Explain Non-Linear Traffic Phenomena. Physica A: Statistical Mechanics and its Applications 385 (2), 667–682.
Payne, H., 1971. Models of freeway traffic and control. *Simulation Council Proceedings*, Mathematical models of public systems 51–61.
Ponnu, B., Coifman, B., 2015. Speed-Spacing Dependency on Relative Speed from the Adjacent Lane: New Insights for Car Following Models. Transportation Research-Part B 82, 74–90.
Ponnu, B., Coifman, B, 2017. When adjacent lane dependencies dominate the uncongested regime of the fundamental relationship. Transportation Research Part B 104, 602–609.
Qian, Z.S., Li, J., Li, X., Zhang, M., Wang, H., 2017. Modeling Heterogeneous Traffic Flow: A Pragmatic Approach. Transportation Research Part B: Methodological 99, 183–204.
Richards, P., 1956. Shock Waves on the Highway. Operations Research 4 (1), 42–51.
Skabardonis, A., Petty, K., Noeimi, H., Rydzewski, D., Varaiya, P., 1996. I-880 Field Experiment: Data-Base Development and Incident Delay Estimation Procedures. *Transportation Research Record 1554*, TRB 204–212.
van Wageningen-Kessels, F., van Lint, H., Hoogendoorn, S.P., Vuik, K., 2014. New Generic Multiclass Kinematic Wave Traffic Flow Model: Model Development and Analysis of its Properties. Transportation Research Record 2422 (1), 50–60.
van Wageningen-Kessels, F., van Lint, H., Vuik, K., Hoogendoorn, S., 2015. Genealogy of traffic flow models. EURO Journal on Transportation and Logistics 4 (4), 445–473.
Wang, C., Coifman, B., 2008. The Effect of Lane-Change Maneuvers on a Simplified Car-following Theory. IEEE Transactions on Intelligent Transportation Systems 9 (3), 523–535.
Wardrop, J., 1952. Some Theoretical Aspects of Road Traffic Research. Proc. Inst. Civil Engineers 1 (Part II), 325–362.
Whitham, G., 1974. Linear and Nonlinear Waves. Wiley, New York.
Wong, G.C.K., Wong, S.C., 2002. A Multi-Class Traffic Flow Model–an Extension of LWR Model with Heterogeneous Drivers. Transportation Research Part A: Policy and Practice 36 (9), 827–841.
Wu, L., Coifman, B., 2014. Vehicle Length Measurement and Length-Based Vehicle Classification in Congested Freeway Traffic. Transportation Research Record 2443, 1–11.
Wu, M., Coifman, B., 2019. Quantifying What Goes Unseen in Instrumented and Autonomous Vehicle Perception Sensor Data- A Case Study. Transportation Research Part C 107, 105–119.
Xuan, Y., Coifman, B., 2012. Identifying Lane Change Maneuvers with Probe Vehicle Data and an Observed Asymmetry in Driver Accommodation. ASCE Journal of Transportation Engineering 138 (8), 1051–1061.
Zhang, H.M., 1999. A Mathematical Theory of Traffic Hysteresis. Transportation Research Part B: Methodological 33 (1), 1–23.
Zhang, H.M., 2002. A non-equilibrium traffic model devoid of gas-like behavior. Transportation Research Part B: Methodological 36 (3), 275–290.
Zhang, H.M., Jin, W., 2002. Kinematic Wave Traffic Flow Model for Mixed Traffic. Transportation Research Record 1802 (1), 197–204.